

1N-05  
380446  
46P

# TECHNICAL MEMORANDUM

## X-283

SUBSONIC FLIGHT TESTS OF A 1/7-SCALE RADIO-CONTROLLED MODEL  
OF THE NORTH AMERICAN X-15 AIRPLANE WITH PARTICULAR  
REFERENCE TO HIGH ANGLE-OF-ATTACK CONDITIONS

By Donald E. Hewes and James L. Hassell, Jr.

Langley Research Center  
Langley Field, Va.

CLASSIFICATION CHANGED TO UNCLASSIFIED  
AUTHORITY: NASA TECHNICAL PUBLICATIONS  
ANNOUNCEMENTS NO. 48

EFFECTIVE DATE: MAY 29, 1961

WHI

CLASSIFIED DOCUMENT - TITLE UNCLASSIFIED

This material contains information affecting the national defense of the United States within the meaning of the espionage laws, Title 18, U.S.C., Secs. 793 and 794, the transmission or revelation of which in any manner to an unauthorized person is prohibited by law.

NATIONAL AERONAUTICS AND SPACE ADMINISTRATION  
WASHINGTON

June 1960



██████████

NATIONAL AERONAUTICS AND SPACE ADMINISTRATION

---

TECHNICAL MEMORANDUM X-283

---

SUBSONIC FLIGHT TESTS OF A 1/7-SCALE RADIO-CONTROLLED MODEL  
OF THE NORTH AMERICAN X-15 AIRPLANE WITH PARTICULAR  
REFERENCE TO HIGH ANGLE-OF-ATTACK CONDITIONS\*

By Donald E. Hewes and James L. Hasseli, Jr.

SUMMARY

An investigation of the subsonic stability and control characteristics of an unpowered 1/7-scale model based on the North American X-15 airplane was conducted by using a radio-controlled model launched from a helicopter and flown in free-gliding flight. At angles of attack below about 20° where the model motions represent those of the X-15 airplane, the model was found to be both longitudinally and laterally stable, and the all-movable tail surfaces were found to be very effective. The model could also be flown at much higher angles of attack where the model motions did not necessarily represent those of the airplane because of slight geometrical differences and Reynolds number effects, but these test results are useful in evaluating the effectiveness at these angles of the type of lateral control system used in the X-15 airplane. In some cases, the model was flown to angles of attack as high as 60° or 70° without encountering divergent or uncontrollable conditions. For some flights in which the model was subjected to rapid maneuvers, spinning motions were generated by application of corrective controls to oppose the direction of rotation. Rapid recoveries from this type of motion were achieved by applying roll control in the direction of rotation.

INTRODUCTION

Studies of the subsonic stability and control characteristics of an unpowered airplane configuration based on the North American X-15 airplane which uses the horizontal tail for pitch and roll control and the all-movable vertical tails for yaw control have been made by using dynamically scaled models. Reports on the flight behavior of this

---

\*Title, Unclassified.

██████████

CONFIDENTIAL

configuration flown in the Langley full-scale tunnel are given in references 1 and 2. In order to study the flight behavior for a much larger range of flight conditions than was possible in the wind-tunnel flight tests, an investigation was conducted by using radio-controlled models launched from a helicopter and flown in free-gliding flight. Although the models were flown at angles of attack as low as  $\alpha = 0^\circ$ , the emphasis of this investigation was placed on the flight characteristics in the high angle-of-attack range where stalls, directional divergences, and spins were likely to be encountered.

As discussed in reference 2 the results of force tests indicated that for angles of attack below about  $20^\circ$ , the model had aerodynamic characteristics very similar to those of the X-15 airplane. Inasmuch as the mass characteristics of the model corresponded very closely to those for the full-scale X-15, the flight motions of the model therefore represent those of the airplane for angles of attack below about  $20^\circ$ . For larger angles of attack, however, the static-force-test data indicated that the aerodynamic characteristics were somewhat different. This difference can be attributed to the effects of both Reynolds number and some geometric differences in the fuselage shape. For these larger angles, therefore, the model motions probably are not directly applicable to the full-scale airplane, but these test results are useful in evaluating the effectiveness at these large angles of the type of lateral-control system used in the X-15 airplane.

#### DEFINITION OF TERMS AND SYMBOLS

All velocities, forces, and moments with the exception of lift and drag are presented with respect to the body-axes system originating at the reference center-of-gravity position. (See fig. 1.) The orientation of the body-axes system relative to the earth is defined by the set of Euler angles  $\psi_E$ ,  $\theta_E$ , and  $\phi_E$  illustrated in figure 2.

X,Y,Z	body reference axes (fig. 1)
$X_e, Y_e, Z_e$	earth reference axes (fig. 2)
S	wing area, sq ft
W	weight, lb
b	wing span, ft
$\bar{c}$	wing mean aerodynamic chord, ft

CONFIDENTIAL

$\mu$	relative density factor, $m/\rho S b$
$m$	mass, slugs
$\rho$	mass density of air, slugs/cu ft
$u, w, v$	components of free-stream velocity, ft/sec
$V$	free-stream velocity, $\sqrt{u^2 + w^2 + v^2}$ , ft/sec
$\alpha$	angle of attack, deg
$\beta$	angle of sideslip, deg
$\dot{\beta} = \frac{d\beta}{dt}$	
$\psi_E$	Euler angle of yaw (azimuth angle), deg
$\phi_E$	Euler angle of roll (bank angle), deg
$\theta_E$	Euler angle of pitch, deg
$p$	rolling velocity about body axis, deg/sec or radians/sec
$q$	pitching velocity about body axis, deg/sec or radians/sec; dynamic pressure, lb/sq ft
$r$	yawing velocity about body axis, deg/sec or radians/sec
$k$	reduced frequency parameter, $\omega b/2V$
$\omega$	circular frequency, radians/sec
$t$	time, sec
$\delta_a$	differential-roll-control deflection, $\delta'_{h_R} - \delta'_{h_L}$ , deg
$\delta_r$	deflection of all-movable vertical tails, positive with trailing edge left, deg
$\delta_h$	pitch-control deflection, $\frac{\delta'_{h_R} + \delta'_{h_L}}{2}$ , deg
$\delta'_h$	deflection of either all-movable horizontal tail, positive with trailing edge down, deg

$F_L$	lift, lb
$F_D$	drag, lb
$F_D'$	component of drag in XZ plane, $F_D \cos \beta$ , lb
$F_Y$	side force, lb
$M_Y$	pitching moment, ft-lb
$M_X$	rolling moment, ft-lb
$M_Z$	yawing moment, ft-lb
$C_L$	lift coefficient, $F_L/qS$
$C_D'$	drag coefficient, $F_D'/qS$
$C_Y$	side-force coefficient, $F_Y/qS$
$C_m$	pitching-moment coefficient, $M_Y/qS\bar{c}$
$C_l$	rolling-moment coefficient, $M_X/qSb$
$C_n$	yawing-moment coefficient, $M_Z/qSb$

$$C_{Y\beta} = \frac{\partial C_Y}{\partial \beta}, \text{ per deg}$$

$$C_{n\beta} = \frac{\partial C_n}{\partial \beta}, \text{ per deg}$$

$$C_{Y_p} = \frac{\partial C_Y}{\partial \frac{pb}{2V}}, \text{ per radian}$$

$$C_{n_p} = \frac{\partial C_n}{\partial \frac{pb}{2V}}, \text{ per radian}$$

$$C_{Y_r} = \frac{\partial C_Y}{\partial \frac{rb}{2V}}, \text{ per radian}$$

$$C_{n_r} = \frac{\partial C_n}{\partial \frac{rb}{2V}}, \text{ per radian}$$

$$C_{Y\dot{\beta}} = \frac{\partial C_Y}{\partial \dot{\beta}}, \text{ per radian}$$

$$C_{n\dot{\beta}} = \frac{\partial C_n}{\partial \dot{\beta}}, \text{ per radian}$$

$$C_{Y\delta_a} = \frac{\partial C_Y}{\partial \delta_a}, \text{ per deg}$$

$$C_{n\delta_a} = \frac{\partial C_n}{\partial \delta_a}, \text{ per deg}$$

$$C_{Y\delta_r} = \frac{\partial C_Y}{\partial \delta_r}, \text{ per deg}$$

$$C_{n\delta_r} = \frac{\partial C_n}{\partial \delta_r}, \text{ per deg}$$

$$C_{l\beta} = \frac{\partial C_l}{\partial \beta}, \text{ per deg} \qquad C_{l\dot{\beta}} = \frac{\partial C_l}{\partial \dot{\beta}}, \text{ per radian}$$

$$C_{l_p} = \frac{\partial C_l}{\partial \frac{pb}{2V}}, \text{ per radian} \qquad C_{l_{\delta a}} = \frac{\partial C_l}{\partial \delta_a}, \text{ per deg}$$

$$C_{l_r} = \frac{\partial C_l}{\partial \frac{rb}{2V}}, \text{ per radian} \qquad C_{l_{\delta r}} = \frac{\partial C_l}{\partial \delta_r}, \text{ per deg}$$

$I_X$             moment of inertia about X body axis, slug-ft<sup>2</sup>

$I_Y$             moment of inertia about Y body axis, slug-ft<sup>2</sup>

$I_Z$             moment of inertia about Z body axis, slug-ft<sup>2</sup>

Subscripts:

L,R            pertaining to left and right directions

U,D            pertaining to up and down directions


H              horizontal tail

V,u            upper vertical tail

V,l            lower vertical tail

### FLIGHT TEST TECHNIQUE

The investigation was made by using a recently developed radio-control technique which consists of launching an unpowered, dynamically scaled model from a helicopter, controlling the model from remote-control ground stations during the gliding flight, and recovering the model by means of a parachute at the end of the flight. The controlled and uncontrolled motions of the model during flight are recorded by means of motion-picture cameras located on the ground, in the helicopter, and in the model. Evaluation of the flight behavior is based on the pilots' observations and the quantitative measurements taken from the motion-picture records. A report of a similar application of this technique to a study of the spinning characteristics of airplane configurations is given in reference 3.


  
Flight Test Facility and Equipment

The flight tests were conducted at an isolated airport near West Point, Virginia. For most of the tests, two ground control stations located about 1,500 feet apart were used, one for the pilot who operated the pitch controls and one for the pilot operating the roll and yaw controls. (See fig. 3.) In some tests, the roll-yaw pilot was located in the helicopter.

Each ground station was provided with communication equipment, a radio-control transmitter, and a motorized tracking unit equipped with a telephoto motion-picture camera and binoculars to assist the pilot in viewing the model. In order to assist in analysis of the test results, magnetic tape recorders were used to record all communicated information and control signals. All phases of the operation were directed by a coordinator located at one of the ground stations.

Radio-control equipment.- The radio-control system consisted of two receivers installed in the model and two audio-tone modulated transmitters located one at each control station. The transmitter at the roll-yaw station consisted of a five-channel unit which provided "on-off" type command signals for aileron and rudder controls and parachute release. Aileron and rudder commands could be given either individually or simultaneously at the discretion of the pilot. The pitch-control transmitter consisted of a three-channel unit which provided up and down pitch-command signals as well as an additional parachute-release signal. A photograph of the radio-control equipment used in the model is shown in figure 4. The model was provided with control-surface actuators which moved the surfaces rapidly through prefixed angular deflections in either direction from the trim or neutral positions in response to the control signals. For most of the tests pneumatic-electric actuators were used, but these were later replaced by all-electric servomechanisms which provided the same type of flicker or "on-off" control action with a greater degree of reliability and simplification. In addition to the flicker action provided for the pitch control, a trimming action was provided for most of the tests by an electrically driven screwjack-type actuator which caused the horizontal-tail surfaces to trim at a constant rate in the direction in which the pitch command was being given. This feature permitted the model to be trimmed over a relatively large angle-of-attack range and still be controlled with small deflections of the surfaces while correcting for small disturbances. Examples of the types of control signals and control-surface responses are illustrated in figure 5. No automatic-stabilization system was provided in the model for this investigation.

The recovery parachute could be released for landing the model at any time during the drop by a command signal from either of the two control stations. In order to provide a fail-safe feature, the parachute





was released automatically whenever the five-channel receiver or transmitter failed to operate satisfactorily.

Construction and instrumentation of the model.- A three-view drawing and a photograph of the model configuration which was similar to the final X-15 configuration (configuration 3) are given in figures 6 and 7, and a list of pertinent geometric characteristics is given in table I. The principal departures from exact scaling of the X-15 airplane are in the fuselage diameter and nose shape. Two identical models constructed of 1/8-inch-thick fiberglass-reinforced plastic were built with molds prepared from the model of the original configuration used in the investigation reported in reference 1. The later configuration changes of the airplane were simulated by reshaping the fuselage side fairings and using the redesigned tail surfaces as discussed in reference 2. Provisions were made so that the model could be flown both with and without the movable portion of the lower vertical tail.

A simplified instrument installation was used to provide sufficient recorded information to obtain a qualitative analysis of the model flight behavior. A 16-mm motion-picture camera using a 17-mm wide-angle lens was installed in the model with a system of mirrors which permitted a picture to be taken through the transparent cockpit canopy. Some of the tests were made with a double-mirror system which provided both a forward and a rearward view, but for later tests this was replaced by a single-mirror system which provided the same view as would be seen by the pilot in the actual airplane. A boom with two swivelling air vanes used to indicate the airspeed and the angles of attack and sideslip was attached to the nose of the model and placed so that the positions of the vanes could be recorded by the camera. Details of these vanes are shown in figure 8 and discussed in the appendix. The positions of the two horizontal-tail surfaces were recorded by the camera by means of two small "fingers" or indexes in the view of the camera and linked directly to the surfaces.

Helicopter and launching equipment.- The helicopter used for launching the model was provided with a special launching rig fitted into the hatch in the floor of the passenger compartment. This rig consisted of a mounting frame fastened to the floor and a retractable strut which lowered the model about 5 feet into relatively smooth air below the helicopter. A mounting fixture provided with a release mechanism was attached to the lower end of the strut to hold the model in a fixed attitude relative to the strut.

A photograph of the model mounted on the helicopter is given in figure 9. The model was stowed below the helicopter in a tail-first attitude in order to obtain sufficient ground clearance for the vertical tails and was mounted so that the angle of attack of the model was about

0° when released. Prior to the launching of the model, the strut was lowered and rotated so that the model headed directly into the wind.

The flight of the model as seen from the helicopter was recorded by a 16-mm motion-picture camera equipped with a 4-inch telephoto lens and operated by a second person located in the helicopter.

Tracking equipment.- A special, motorized tracking unit, shown in figure 10, used at each control station consisted of a modified machine-gun mount equipped with a bucket seat for the pilot of the model. A pair of  $7\frac{1}{2}$ -power binoculars were used for viewing the model, and an adjustable mount for these was provided in order to free the pilot's hands for operating the transmitter controls.

L  
9  
0  
8

The tracking operator used the standard gunsight and controls to keep the tracking unit aligned with the model. A telephoto motion-picture camera mounted to the unit was operated by the tracking operator to record the flight of the model.

Retrieving equipment.- The retrieving system for the model consisted of a standard 12-foot-diameter cargo parachute attached to the model with shock-absorbing nylon webbing. The parachute was stored in an aluminum can in the rear of the model and extracted by means of a small spring-loaded pilot parachute.

#### Model Flight Tests

Flight conditions simulated in the tests of the dynamic models corresponded to those for the full-scale airplane flying subsonically both with and without the lower vertical tail at approximately 19,000 feet altitude with a gross weight of 12,546 pounds and with the landing gear and flaps retracted. Mass characteristics of the two models were identical and were scaled from those for the full-scale airplane on the basis of a constant Froude number. Dynamic scaling in this manner maintains the proper relation between linear and angular accelerations, and as a result the time histories of the model motions correspond exactly to those for the airplane when the linear distances and the time scale are expanded by factors equal to the scaling factor, in this case 7, and the square root of this factor, respectively. A list of the mass characteristics, control-surface settings, and deflections used in the tests is given in table II, and a comparison of the model and airplane mass characteristics is shown in table III. The Reynolds number based on  $\bar{c}$  for these tests was in the order of  $0.7 \times 10^6$ ; whereas the corresponding full-scale value is about  $11 \times 10^6$ .

The model was trimmed for about zero lift and was released from the helicopter at an airspeed of about 40 knots and an altitude of between 1,500 and 2,000 feet. Three to four seconds after release, the horizontal tails were deflected to trim the model to a high angle of attack and the "roll-yaw" or "lateral" pilot attempted to fly the model along a pre-scribed flight path and to recover the model from any uncontrolled maneuvers which occurred.

#### DATA REDUCTION

Analysis of the flight behavior of the model was based on the pilots' observations and comments and on quantitative measurements of the following variables taken from the motion-picture records:

V, ft/sec . . . . .	±5
$\alpha$ , deg . . . . .	±4
$\beta$ , deg . . . . .	±4
$\theta_E$ , deg . . . . .	±10
$\psi_E$ , deg . . . . .	±10
$\phi_E$ , deg . . . . .	±10
p, deg/sec . . . . .	±10
q, deg/sec . . . . .	±10
r, deg/sec . . . . .	±10
$\delta_a$ , deg . . . . .	±2
$\delta_h$ , deg . . . . .	±2
$\delta_r$ , deg . . . . .	±2
t, sec . . . . .	±0.5

The measurements were believed to be accurate within the limits given in the table. While some of these values were rather inaccurate for purposes of extracting aerodynamic parameters, these measurements permitted the preparation of time histories which were useful in qualitative analysis of the stability and control response characteristics of the model.

The basic time reference for the flight records was the model camera speed of 32 frames per second regulated by a built-in governor. The various other film records of a given flight were correlated with the model camera on the basis of the time interval from moment of release of the model to the instant of parachute deployment. The flight histories of the models are presented in the report on the basis of true time for the model, and the motions of the model correspond to those for the full-scale airplane when presented on the basis of a time scale equal to  $\sqrt{7}$  times that for the model. A discussion of the methods for obtaining the quantitative measurements is presented in the appendix.

## STABILITY AND CONTROL PARAMETERS OF THE MODEL

The aerodynamic characteristics of the models for an angle-of-attack range from  $0^\circ$  up to at least  $60^\circ$  as determined from wind-tunnel tests are presented in references 2 and 4. For convenience in discussing results of this investigation, some of the pertinent data from these references are presented in figures 11 to 14 and are reviewed briefly.

The data of figure 11(a) indicate that for zero sideslip the model configuration was longitudinally stable for all values of trimmed lift coefficients (that is, the lift coefficients for  $C_m = 0$ ). With a pitch-control deflection  $\delta_h$  of  $-30^\circ$ , the configuration was trimmed at an angle of attack of about  $50^\circ$ . Some unpublished data presented in figure 11(b) showing the variations of pitching moment with angle of attack for several different angles of sideslip indicate that the trim angle of attack for  $\delta_h = -30^\circ$  varies from about  $36^\circ$  to  $57^\circ$  for values of  $\beta$  between  $\pm 30^\circ$ . A cross plot of the data of figure 11(b) is presented in figure 11(c) and reveals that the variations of the pitching moment due to sideslipping are fairly symmetrical about  $\beta = 0^\circ$  for angles of attack from  $0^\circ$  to about  $30^\circ$ ; whereas they are asymmetrical for larger values of  $\alpha$ . This asymmetry is explained by the same phenomenon which causes the asymmetrical yawing moments discussed in reference 2. Essentially, this asymmetry results from a large vortex shed from one side of the fuselage nose, and both the yawing and pitching moments are components of a resultant moment generated by the distorted air-flow pattern. The significance of this effect is that large interactions between the longitudinal and lateral modes of motion can occur in this angle-of-attack range as a result of control input, airstream gust input, or initial motion.

The horizontal tails when operated differentially maintained effectiveness as a roll control for angles of attack up to at least  $50^\circ$  as illustrated in figure 12(a) which shows the variation of the lateral-control-effectiveness parameters with trim angle of attack. The yawing moments produced by the roll control were favorable up to about  $\alpha = 35^\circ$  to  $40^\circ$  and became unfavorable at high angles. It should be pointed out that in the flight tests trim conditions did not always exist and these data therefore are not applicable in some cases. (Untrimmed control effectiveness data for various elevator settings are available in ref. 2.)

Effectiveness of the all-movable vertical tails as a rudder or yaw control decreased almost uniformly with increasing angle of attack, becoming zero at about  $\alpha = 43^\circ$  for the complete configuration and at about  $\alpha = 55^\circ$  for the model with the lower rudder off. (See fig. 12(b).)

As indicated in figure 13, the model configuration with the lower rudder on was directionally stable for small sideslip angles and for angles of attack up to about  $\alpha = 18^\circ$  and also between about  $\alpha = 30^\circ$  and  $\alpha = 60^\circ$ . With the lower rudder off, the configuration was directionally stable for angles up to about  $\alpha = 17^\circ$  and was unstable for all higher angles.

Effective dihedral of the model configuration was positive for small sideslip angles and for an angle-of-attack range up to about  $17^\circ$  and also above about  $43^\circ$ .

Figure 14 shows the variation of some of the stability parameters measured in dynamic force tests where the model was oscillated in roll and yaw. (See ref. 4.) These data are quite similar for the model both with and without the lower rudder. The aerodynamic damping both in roll and yaw is positive throughout the angle-of-attack range and increases markedly in the range of angles near  $\alpha = 30^\circ$ .

## RESULTS AND DISCUSSION

The details of five typical flight tests are described briefly to indicate the significant results obtained from the complete series of tests. The motion-picture records of each of these tests are presented in a film supplement to this report. A request card form and a description of the film will be found at the back of this paper, on the page immediately preceding the abstract and index pages. Some of the test conditions for these tests are given in table II, and time histories of the model motions are given in figures 15 to 19.

The following table gives the five flight tests discussed in this report:

Test	Configuration	Type of test	Figure
A	Lower rudder off	Stability and control at low angles of attack ( $\alpha < 20^\circ$ )	15
B	Lower rudder off	Stability and control at high angles of attack (average $\alpha = 60^\circ$ )	16
C	Lower rudder off	Incipient spin and recovery	17
D	Lower rudder on	Stability and control at high angles of attack	18
E	Lower rudder on	Incipient spin and recovery	19

## Flight Test A

Flight test A illustrates the stability and control characteristics of the model at relatively low angles of attack (generally below about  $20^\circ$ ) with the use of only the roll control for lateral maneuvering (fixed rudder) and with the lower rudder removed to give the minimum directional stability. The time histories of the measured quantities for this test are presented in figure 15. After the model was launched, it flew briefly at about  $\alpha = 0^\circ$ ; and then as the pitch control was deflected from  $\delta_h = 1^\circ$  to  $-11^\circ$  the roll pilot maneuvered the model through a series of banking maneuvers. Response to the roll and pitch controls and both longitudinal and lateral stability of the model were satisfactory. These results are in qualitative agreement with those reported in reference 2 for the model flown in the full-scale tunnel with the lower rudder off.

## Flight Test B

Flight test B illustrates the stability and control of the model at high angles of attack for about the same conditions as for test A. The time histories of the measured quantities for this test are presented in figure 16. Initially, while the angle of attack was relatively low, the roll pilot was able to hold the model in the intended heading using very short "bursts" or "flicks" of the control stick indicating the control response at the low angles of attack was satisfactory, as in the case of test A. As higher angles of attack were reached, however, the duration of roll control applied to maintain heading increased up to the point at which the control was being held almost continuously indicating very weak control response for these larger angles; that is, for angles above about  $40^\circ$ . It should be noted that the full application of left roll control produced very little bank angle but did produce an appreciable left sideslip angle. This poor control response is attributed to the relatively large adverse yawing moments produced by the roll control at these angles (see fig. 12(a)) combined with the positive effective dihedral at these angles of attack (fig. 13). This combination of characteristics produces an adverse rolling moment that opposes the rolling moment produced by the roll control.

The record of the sideslip angle reveals a tendency for the model to fly sideslipped to the left at the high angles of attack since the average value of  $\beta$  while left roll control was being applied is in the order of  $-10^\circ$  or  $-12^\circ$  and was about  $0^\circ$  with right control. This sideslipping tendency is attributed to the asymmetrical moments acting on the model as discussed earlier.

The time history for this test indicates that the model had a sustained longitudinal oscillation with an amplitude of about  $\alpha = \pm 20^\circ$

and a relatively long period of about 2.5 seconds with the horizontal tail trimmed to its maximum negative deflection. The average angle of attack was about  $60^\circ$ . A lightly damped oscillatory rolling mode existed at these large angles as evidenced by the sideslip angle and bank attitude traces. The amplitude of this oscillation was in the order of  $\phi_E = \pm 10^\circ$  with a period of about 0.8 second. It is possible that each cycle of longitudinal motion tended to produce a roll disturbance which sustained the lightly damped rolling mode. The pilots made no attempt to control or damp either the longitudinal or lateral oscillations. It is significant to note that although these motions did not appear to be heavily damped and force-test data showed that the model was directionally unstable at the high angles of attack, the model did not exhibit any rapid divergent tendencies and could be maneuvered slowly with the limited amount of roll control available. Lateral stability of the model at these high angles of attack is attributed primarily to the fact that the effective dihedral ( $-C_{l\beta}$ ) is positive in this angle-of-attack range. (See fig. 13.)

#### Flight Test C

Flight test C illustrates the entrance into a spinning motion resulting from an attempt to keep the wings level and to maintain a given heading with roll control as the model was pulling out of a dive. (See fig. 17.) The model was flown with about the same conditions as for tests A and B. Although a slightly larger maximum horizontal-tail incidence was used in this flight, the transient motions, which are of interest in this test, occurred before this maximum setting was reached; therefore the maximum setting had no significance.

The time histories for this test indicate that the roll pilot applied left control to correct the model heading after the launch when the angle of attack was at about  $12^\circ$  and the model was diving. The response was very rapid and produced a steep bank to the left; immediately a corrective right control was applied to raise the low wing. Shortly thereafter as the model banked into a right turn, the horizontal tail was deflected to bring up the nose. As the model pitched up in response to this pitch control, left control was applied to oppose the right turn; and immediately the angle of attack, which had reached a peak of  $\alpha = 50^\circ$ , increased to above  $80^\circ$  with no apparent effect on the rate of turn, which reached about 160 deg/sec. The angle of attack oscillated between about  $60^\circ$  and  $90^\circ$  with a period of about 1.5 seconds as the model continued to rotate for a total of about three turns. A rolling oscillation with about the same period and with an amplitude of approximately  $\phi_E = \pm 10^\circ$  is evident in the bank-attitude record. These high angle-of-attack conditions correspond to those of a spin with the roll control applied in the direction to promote the spin as discussed in reference 5. Inasmuch as this reference states that up to five turns

CONFIDENTIAL

are required to attain a fully developed spin, this motion is referred to as an incipient spinning motion.

After three turns the roll controls were deflected to the right or in the direction of the spin, as recommended in reference 5 for fully developed spin recovery, and the rotation ceased very abruptly with the angle of attack dropping toward zero, indicating that the type of control used was very effective in recovering from this incipient spinning motion. The angle of attack increased to above  $40^\circ$  after the recovery because the horizontal-tail incidence was still large, but the model did not reenter a spin.

It appears that inertial coupling between the longitudinal and lateral modes of motion generated by the pilot's attempt to oppose the turn while the model was pitching up was primarily responsible for the spinning motion. A second factor which perhaps had a significant effect in promoting and sustaining the spin is the asymmetry both in pitch and yaw discussed previously.

#### Flight Test D

Flight test D illustrates the stability and control of the model with the lower rudder on at high angles of attack, and the results are somewhat similar to those for the flight test B in which the lower rudder was removed. The roll control response at the large angles of attack was very poor as indicated in figure 18 by the continuous left control applied to overcome the right turn. The figure shows that the roll control produced very little bank angle and excessive adverse sideslip for the same reason as pointed out for flight test B.

The oscillatory condition indicated by both the sideslip and angle of bank records appears to be more predominant for this test than for test B. The  $\beta$  record indicates a general tendency for the oscillation to damp at the higher angles of attack and to build up where  $\alpha$  is in the order of  $40^\circ$  to  $50^\circ$ . The period of the lateral oscillation is about the same as shown previously in test B.

The curves for damping in roll presented in figure 14 show that, near  $\alpha = 50^\circ$  with the lower rudder on, the damping decreases rapidly as  $\alpha$  is varied; whereas with the rudder off the damping decreases only gradually. The lower rudder, therefore, appears to have had an adverse effect on the rolling mode as the result of reduced damping in roll near  $\alpha = 50^\circ$ . It should be noted that although this rolling mode was evident, the lateral motion did not actually diverge enough to cause the model to perform any violent and uncontrollable maneuvers.

CONFIDENTIAL



## Flight Test E

Flight test E was made with both the upper and lower rudders on, and through the latter part of the flight the rudders were deflected in the sense opposite to the roll control, that is, crossed lateral control. (See fig. 19.)

In this test, the pilot applied right roll control to overcome the steep banked turn to the left at the same time as the pitch control was deflected up. This action, similar to that discussed for test C, brought about the rapid increase in  $\alpha$  to a value in the order of  $70^\circ$  and resulted in a spin with a rate of about 100 deg/sec, which is considerably lower than that of test C. Application of the crossed lateral control in the direction to promote the spin had no apparent immediate effect on this incipient spinning motion. Reversing the direction of the crossed lateral control caused the model to bank to the left and to recover very rapidly from the spinning maneuver.

The most significant difference between tests C and E, aside from the direction of spin, is that the rate of spin rotation with the lower rudder on was much lower than with it off indicating the lower rudder tends to damp or oppose the spin. It appears that the direction of divergence into the spin was determined by the direction of bank at the time the elevator and lateral control were applied.

## CONCLUDING REMARKS

The following conclusions were drawn from the results of the investigation of the subsonic stability and control characteristics of an unpowered radio-controlled model based on the X-15 configuration with all-movable tail surfaces for longitudinal and lateral control by using radio-controlled models:

1. In general, the testing technique utilizing radio-controlled models appears to be satisfactory for studying the flight behavior of airplane configurations at high angles of attack.
2. The model was longitudinally and laterally stable, and the all-movable controls were very effective for relatively low angles of attack below about  $\alpha = 20^\circ$ , where the model motions represent those of the X-15 airplane.
3. The model could be flown at much higher angles of attack, where the model motions did not necessarily represent those of the airplane because of slight geometrical differences and Reynolds number effects,

~~CONFIDENTIAL~~

and in some cases the model was flown to angles of attack as high as  $60^{\circ}$  to  $70^{\circ}$  without encountering divergent or uncontrollable conditions.

4. For other flights, in which the model was subjected to rapid maneuvers involving positive pitching velocities and corrective lateral-control movements, divergent conditions were encountered. These divergent conditions which were apparently caused by inertial coupling between the longitudinal and lateral modes of motion produced incipient spinning motions. Rapid recoveries from these motions were achieved by applying roll control in the direction of rotation.

Langley Research Center,  
National Aeronautics and Space Administration,  
Langley Field, Va., February 16, 1960.

~~CONFIDENTIAL~~

## APPENDIX

## METHODS FOR OBTAINING QUANTITATIVE MEASUREMENTS

The flight velocity  $V$  of the model was measured by means of one of the two air vanes attached to the nose boom. This vane was free to align itself with the airstream direction at the nose boom and was provided with canted fins which were free to rotate with an angular velocity directly proportional to the resultant airstream velocity. The angular velocity was determined from the model camera film records by measuring the angular displacement of the canted fins between consecutive frames on the film.

Corrections for the velocity increments at the air-vane location due to angular velocities of the model were not applied to the measured values because in most cases the increments were small and were within the limits of accuracy of the basic measurements.

The angles of attack and sideslip as indicated by the second air vane were measured from the model camera film records by use of a duplicate air vane mounted on a calibration jig. The jig was mounted in front of the projection screen and aligned with the axis of the projector lens exactly as the flight-test boom and vanes were aligned with the model camera lens and mirror system. As each frame of the film record was projected on the screen, the position of the duplicate air vane was adjusted so that the shadow corresponded as close as possible with the projected image of the flight-test air vane. Angles of attack and sideslip were read directly from scales on the calibration jig. This procedure eliminated a long and tedious procedure of taking measurements of the image and calculating the angles on the basis of the foreshortened dimensions of the air vane. Corrections to compensate for the angular velocities of the model were not applied to the angles as measured at the end of the nose because, in most cases, these corrections were small and within the accuracy of the basic measurements.

Measurements of the attitude angles  $\theta_E$ ,  $\psi_E$ , and  $\phi_E$  were obtained from the various views taken during the tests. Measurements of  $\psi_E$  were generally obtained from the overhead view as seen from the helicopter while values of  $\theta_E$  and  $\phi_E$  were generally obtained from the model camera records.

Values for the angular velocities  $p$ ,  $q$ , and  $r$ , were obtained from the model camera records by measuring the linear and angular displacements from frame to frame of various objects, such as trees, houses, or

roads, viewed in the background of the film records. This procedure required the assumption that the motion of these objects relative to the axis of the camera is due solely to the angular motions of the model and are independent of linear displacements. The errors introduced by this assumption are very small particularly when the viewed objects are distant, such as a half to one mile away, and are in the direction the model is moving. Briefly, the procedure consisted of drawing a line on the projection screen between two relatively distant and sharply defined objects  $A_1$  and  $B_1$  seen in a given frame, as illustrated in figure 20, and then repeating the process for the same two objects  $A_2$  and  $B_2$  in the next frame. The value of  $p$  was found by measuring the angle  $\Delta\phi$  between the two lines and dividing by the time interval between the two frames, in this case  $1/32$  of a second (32 frames per second is framing speed of camera).

The values for  $q$  and  $r$  were obtained by measuring the angular displacement of an axis of the camera parallel with the X-axis of the model for any two consecutive frames in the film record. The point  $C_1$  represents the intersection of the X-axis with the plane of the picture for the first frame and is determined by the alinement of the camera in the model. In order to determine the displacement (refer to fig. 20), arcs with radii equal to the distances  $A_1C_1$  and  $B_1C_1$  as determined in the first frame were swung from points  $A_2$  and  $B_2$ . The intersection  $C_{1,2}$  of the two arcs established the position of  $C_1$  relative to the second frame. The linear displacements  $z$  and  $y$  as measured on the screen were converted to values of  $q$  and  $r$  by using the following equations:

$$q = (32z)(K) \text{ deg/sec}$$

and

$$r = (32y)(K) \text{ deg/sec}$$

where  $K$  is equal to  $\frac{34^\circ}{y_F}$  or  $\frac{26^\circ}{z_F}$  and  $y_F$  and  $z_F$  are the width and height of the projected frame and the  $34^\circ$  and  $26^\circ$  are the horizontal and vertical angular fields of vision of the model camera.

The control-surface deflections  $\delta_h$ ,  $\delta_a$ , and  $\delta_r$  were determined from records of the control signals and the known preset surface deflections and rates of travel.

## REFERENCES

1. Boisseau, Peter C.: Investigation of the Low-Speed Stability and Control Characteristics of a 1/7-Scale Model of the North American X-15 Airplane. NACA RM L57D09, 1957.
2. Hassell, James L., Jr., and Hewes, Donald E.: Investigation of the Subsonic Stability and Control Characteristics of a 1/7-Scale Model of the North American X-15 Airplane With and Without Fuselage Forebody Strakes. NASA TM X-210, 1960.
3. Libbey, Charles E., and Burke, Sanger M., Jr.: A Technique Utilizing Free-Flying Radio-Controlled Models to Study the Incipient- and Developed-Spin Characteristics of Airplanes. NASA MEMO 2-6-59L, 1959.
4. Paulson, John W., and Hassell, James L., Jr.: Low-Speed Measurements of Oscillatory Lateral Stability Derivatives of a 1/7-Scale Model of the North American X-15 Airplane. NASA TM X-144, 1959.
5. Neihouse, Anshal I., Klinar, Walter J., and Scher, Stanley H.: Status of Spin Research for Recent Airplane Designs. NACA RM L57F12, 1957.

TABLE I.- GEOMETRIC CHARACTERISTICS OF THE NORTH AMERICAN X-15 AIRPLANE (CONFIGURATION 3)  
AND SCALED-UP CHARACTERISTICS OF THE 1/7-SCALE MODEL

[All values are for complete configuration with lower rudder on]

	Scaled-up model values	Full-scale values
<b>Wing:</b>		
Airfoil section . . . . .	NACA 66-005 (modified)	NACA 66-005 (modified)
Area, S, sq ft . . . . .	200	200
Span, b, ft . . . . .	22.36	22.36
Root chord, $c_r$ , ft . . . . .	14.91	14.91
Tip chord, $c_t$ , ft . . . . .	2.98	2.98
Mean aerodynamic chord, $\bar{c}$ , ft . . . . .	10.27	10.27
Fuselage-station number at 0.25 $\bar{c}$ . . . . .	345.86	345.353
Leading-edge sweep, deg . . . . .	36.75	36.75
Trailing-edge sweep, deg . . . . .	-17.75	-17.75
Dihedral, deg . . . . .	0	0
Incidence, deg . . . . .	0	0
Aspect ratio, $b^2/S$ . . . . .	2.50	2.50
Taper ratio, $c_t/c_r$ . . . . .	0.20	0.20
<b>Fuselage:</b>		
Length, ft . . . . .	49.00	49.83
Depth (maximum) basic fuselage, ft . . . . .	4.42	4.67
Width (maximum) including side fairing, ft . . . . .	7.58	7.33
<b>Horizontal tail:</b>		
Airfoil section (parallel to center line) . . . . .	NACA 66-005 (modified)	NACA 66-005 (modified)
Area:		
Total (through fuselage), sq ft . . . . .	110.69	115.34
Exposed (movable), sq ft . . . . .	50.62	52.05
Total span (through fuselage), ft . . . . .	17.63	18.08
Root chord, ft . . . . .	10.02	10.22
Tip chord, ft . . . . .	2.15	2.17
Fuselage chord, ft . . . . .	6.95	7.02
Mean aerodynamic chord, ( $\bar{c}_H$ ) <sub>exposed</sub> , ft . . . . .	4.96	5.00
Fuselage station number at (0.25 $\bar{c}_H$ ) <sub>exposed</sub> , ft . . . . .	524.00	526.000
Leading-edge sweep, deg . . . . .	50.58	50.58
Trailing-edge sweep, deg . . . . .	19.28	19.28
Dihedral, deg . . . . .	-15.00	-15.00
Aspect ratio (based on total area) . . . . .	2.82	2.83
Taper ratio . . . . .	0.21	0.21
Longitudinal distance from 0.25c to (0.25 $\bar{c}_H$ ) <sub>exposed</sub> , ft . . . . .	14.84	15.05
<b>Upper vertical tail:</b>		
Airfoil section . . . . .	10° wedge	10° wedge
Area:		
Total (above fuselage chord line), sq ft . . . . .	40.83	40.83
Movable portion, sq ft . . . . .	26.65	26.65
Span:		
Total (above fuselage chord line), ft . . . . .	4.69	4.69
Movable portion, ft . . . . .	3.16	3.16
Fuselage chord, ft . . . . .	10.16	10.16
Rudder root chord, ft . . . . .	9.36	9.36
Tip chord, ft . . . . .	7.53	7.53
Mean aerodynamic chord, $\bar{c}_{V,u}$ , (based on total area above fuselage chord line), ft . . . . .	9.23	9.23
Fuselage station number at 0.25 $\bar{c}_{V,u}$ . . . . .	493.44	493.44
Leading-edge sweep, deg . . . . .	30.0	30.0
Trailing-edge sweep, deg . . . . .	0	0
Aspect ratio (based on total area above fuselage chord line) . . . . .	0.52	0.52
Taper ratio . . . . .	0.74	0.74
Longitudinal distance from 0.25 $\bar{c}$ to 0.25 $\bar{c}_{V,u}$ , ft . . . . .	12.30	12.34
<b>Lower vertical tail:</b>		
Airfoil section . . . . .	10° wedge	10° wedge
Area:		
Total (below fuselage chord line), sq ft . . . . .	34.48	34.22
Movable (jettisonable) portion, sq ft . . . . .	20.30	19.95
Span:		
Total (below fuselage chord line), ft . . . . .	3.82	3.83
Movable (jettisonable) portion, ft . . . . .	2.33	2.38
Fuselage chord, ft . . . . .	10.21	10.21
Rudder root chord, ft . . . . .	9.37	9.48
Tip chord, ft . . . . .	8.10	7.99
Mean aerodynamic chord, $\bar{c}_{V,l}$ , (based on total area below fuselage chord line), ft . . . . .	9.20	9.17
Fuselage station number at 0.25 $\bar{c}_{V,l}$ , ft . . . . .	491.48	491.483
Leading-edge sweep, deg . . . . .	30.0	30.0
Trailing-edge sweep, deg . . . . .	0	0
Aspect ratio (based on total area below fuselage chord line) . . . . .	0.43	0.43
Taper ratio . . . . .	0.78	0.78
Longitudinal distance from 0.25 $\bar{c}$ to 0.25 $\bar{c}_{V,l}$ , ft . . . . .	12.12	12.18

TABLE II.- MASS CHARACTERISTICS AND CONTROL-SURFACE DEFLECTIONS FOR THE FLIGHT TESTS

Flight test	Weight, lb	W/S, lb/sq ft	Center of gravity	I <sub>x</sub> , slug-ft <sup>2</sup>	I <sub>y</sub> , slug-ft <sup>2</sup>	I <sub>z</sub> , slug-ft <sup>2</sup>	δ <sub>h</sub> '		δ <sub>r</sub> , deg	δ <sub>h</sub> trim, deg	δ <sub>h</sub> trim rate, deg/sec
							Roll, deg	Pitch, deg			
A	66.5	16.3	0.209ē	0.460	7.90	8.03	±7.5	±6	0	-5	0
B	66.5	16.3	.209ē	.460	7.90	8.03	±6.0	±4	0	0 to -28	5.0
C	66.5	16.3	.209ē	.460	7.90	8.03	±7.5	±6	0	-5 to -35	4.3
D	67.0	16.4	.214ē	.463	7.92	8.08	±7.0	±6	0	-5 to -35	4.4
E	67.0	16.4	.214ē	.463	7.92	8.08	±10.0	±5	±5	-5 to -36	4.4

TABLE III.- COMPARISON OF MASS CHARACTERISTICS OF THE MODEL AND FULL-SCALE AIRPLANE

[Values for the model with lower rudder on are presented in terms of full-scale values]

	Altitude, ft	Weight, lb	ρ	μ	I <sub>x</sub>	I <sub>y</sub>	I <sub>z</sub>
Model (actual)	0	22,850	0.00238	67	7,730	132,700	135,200
Model (simulated)	19,000	12,550	.00130	67	4,230	72,600	74,000
Airplane	19,000	12,546	.00130	67	3,378	73,726	75,246

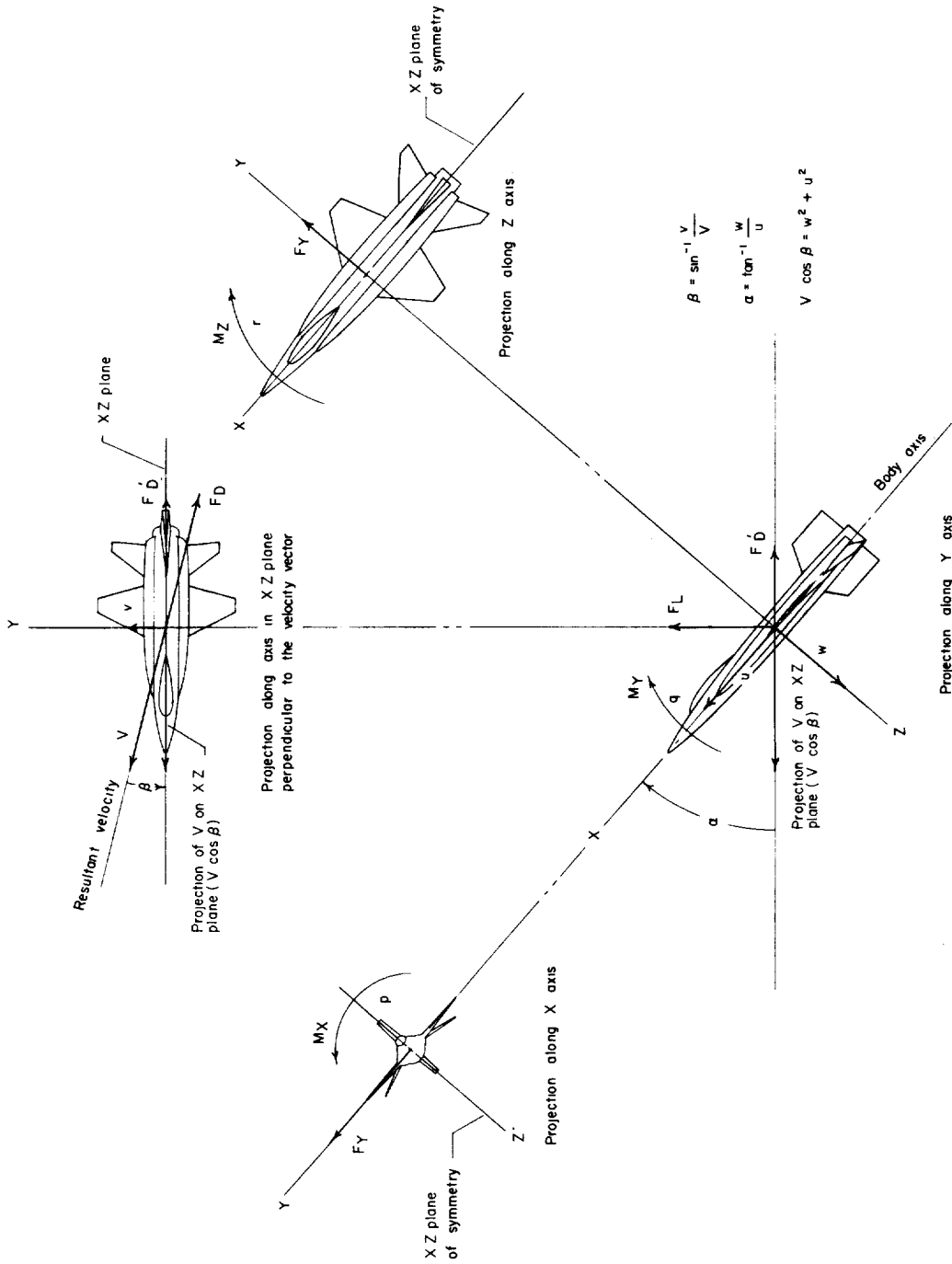


Figure 1.- Body system of axes. Arrows indicate positive directions of moments, forces, angles, and velocities.

CONFIDENTIAL



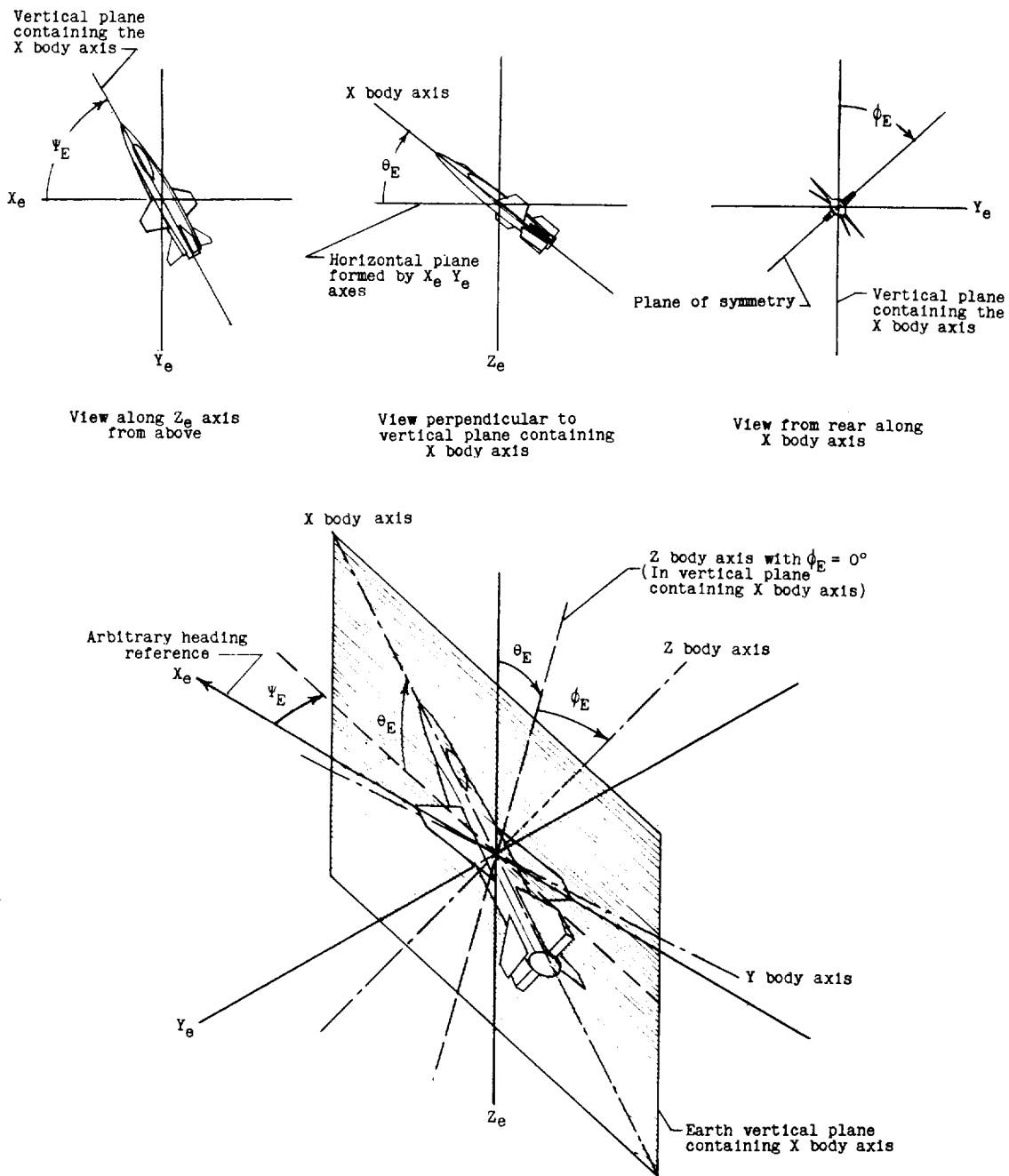


Figure 2.- Orientation of body system of axes relative to the earth.

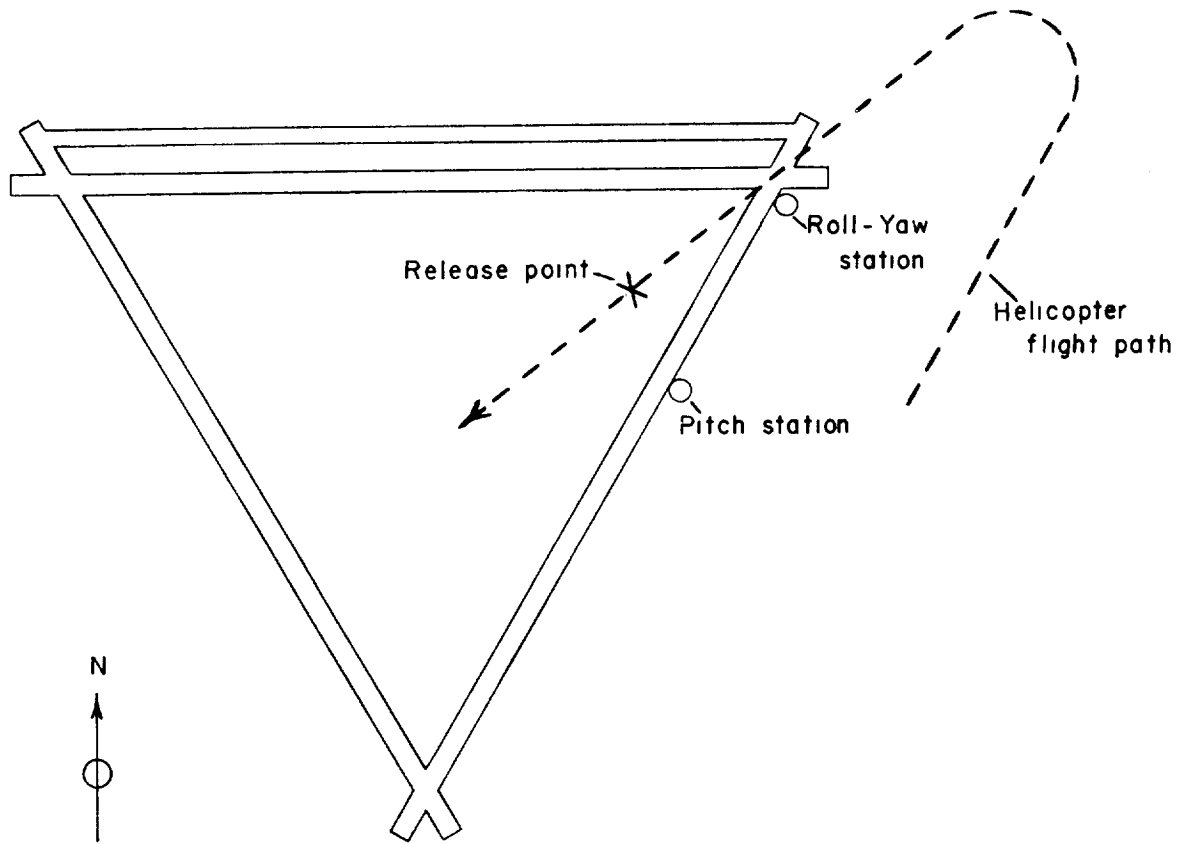


Figure 3.- Diagram of test site.



Figure 4.- Model radio equipment. L-57-1666

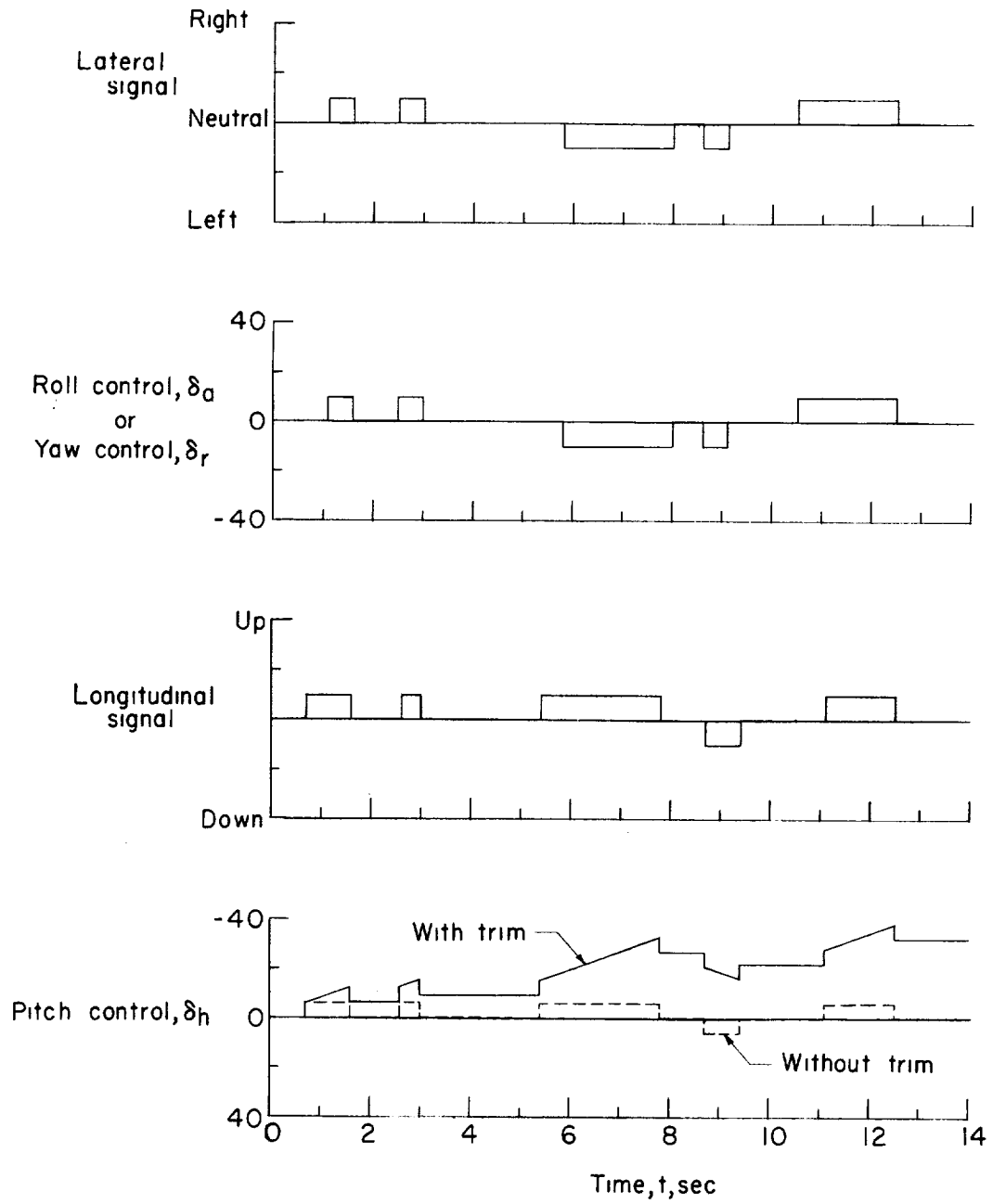


Figure 5.- Sketch illustrating control signals and corresponding control-surface movements.



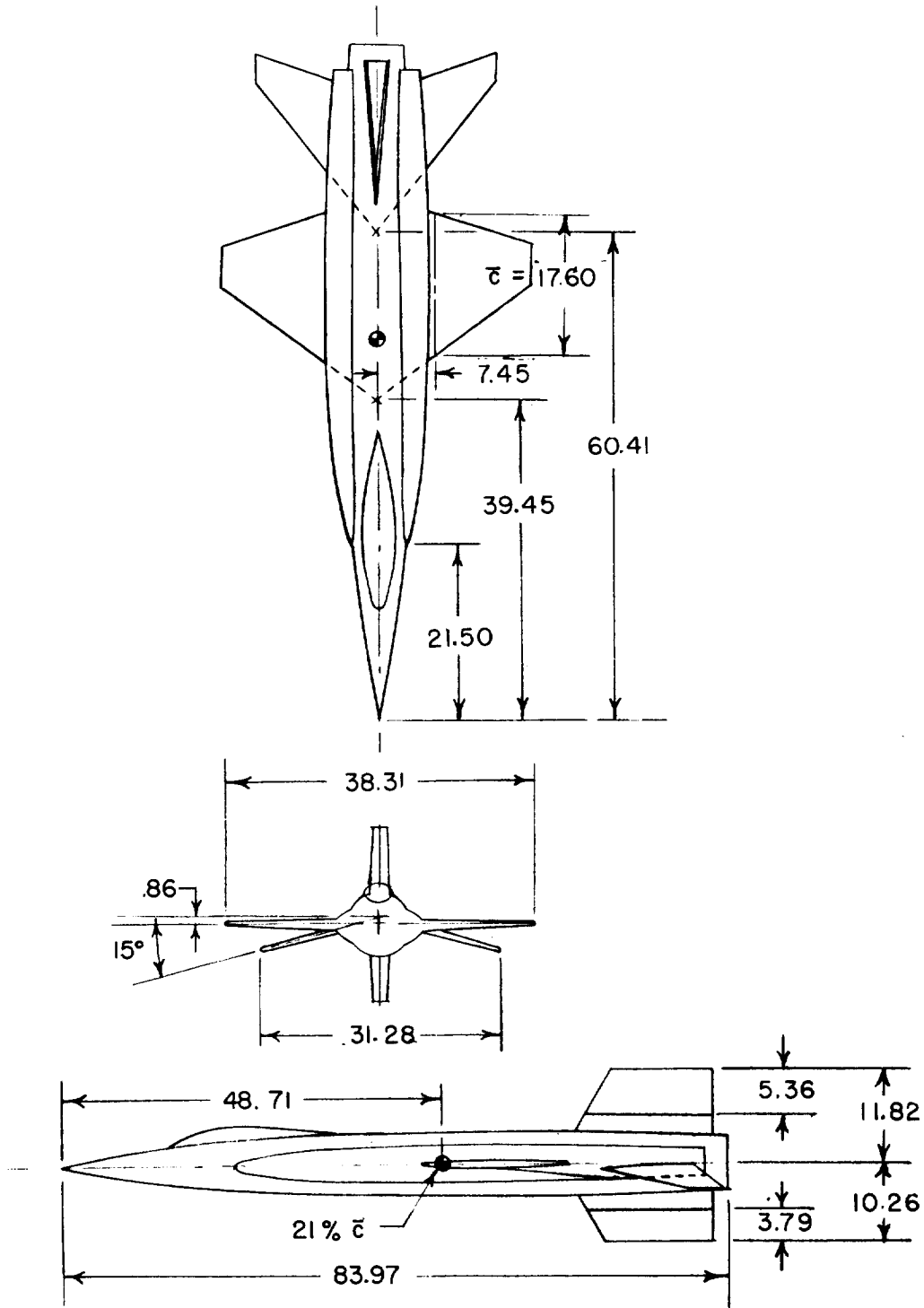
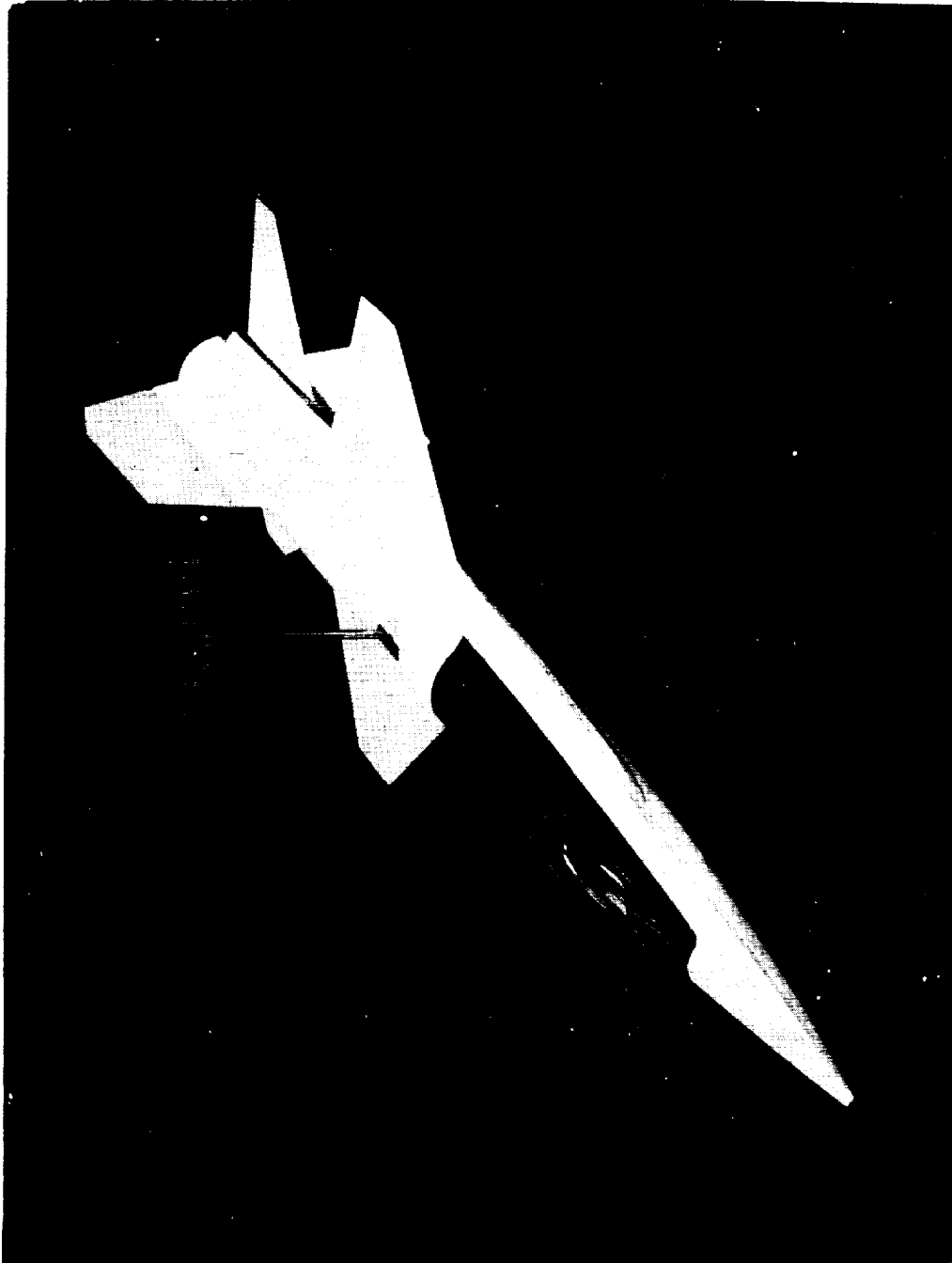


Figure 6.- Three-view drawing of 1/7-scale model of the X-15. All dimensions are in inches.

~~CONFIDENTIAL~~



L-57-5546

Figure 7.- Photograph of the X-15 model.

~~CONFIDENTIAL~~

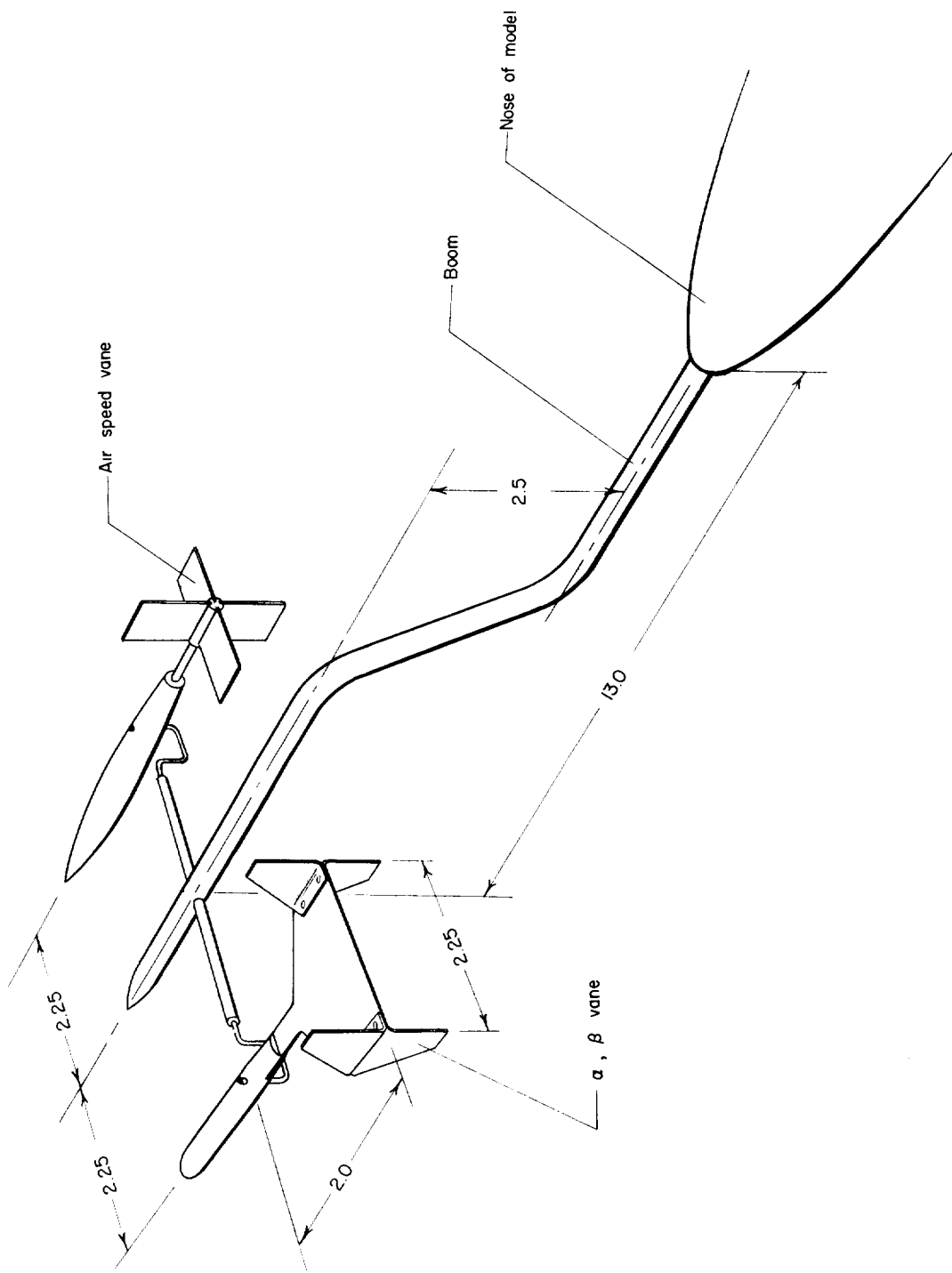


Figure 8.- Sketch of air vanes.

~~CONFIDENTIAL~~



L-57-1468  
Figure 9.- Photograph of model attached to helicopter launch rig.

~~CONFIDENTIAL~~



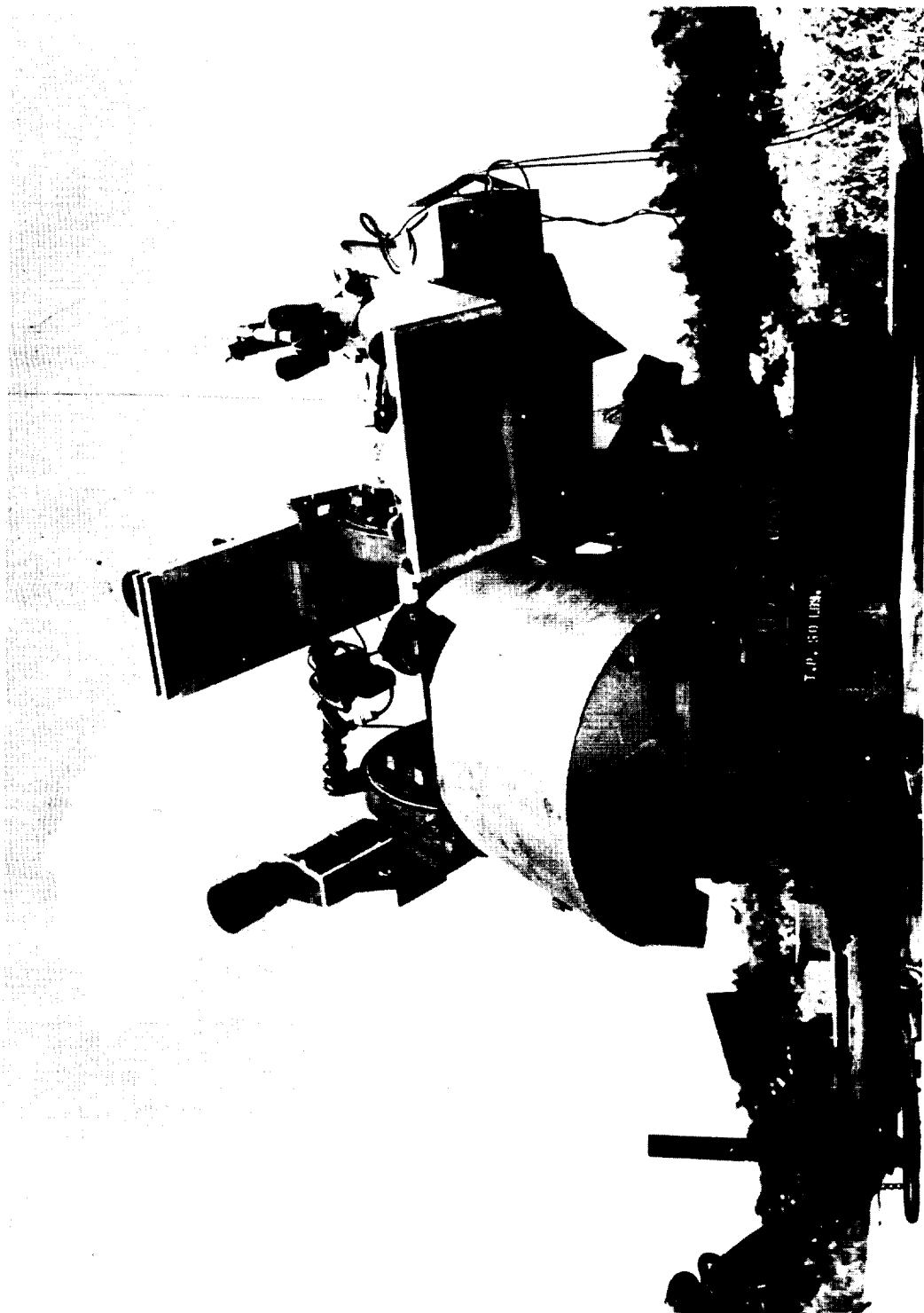
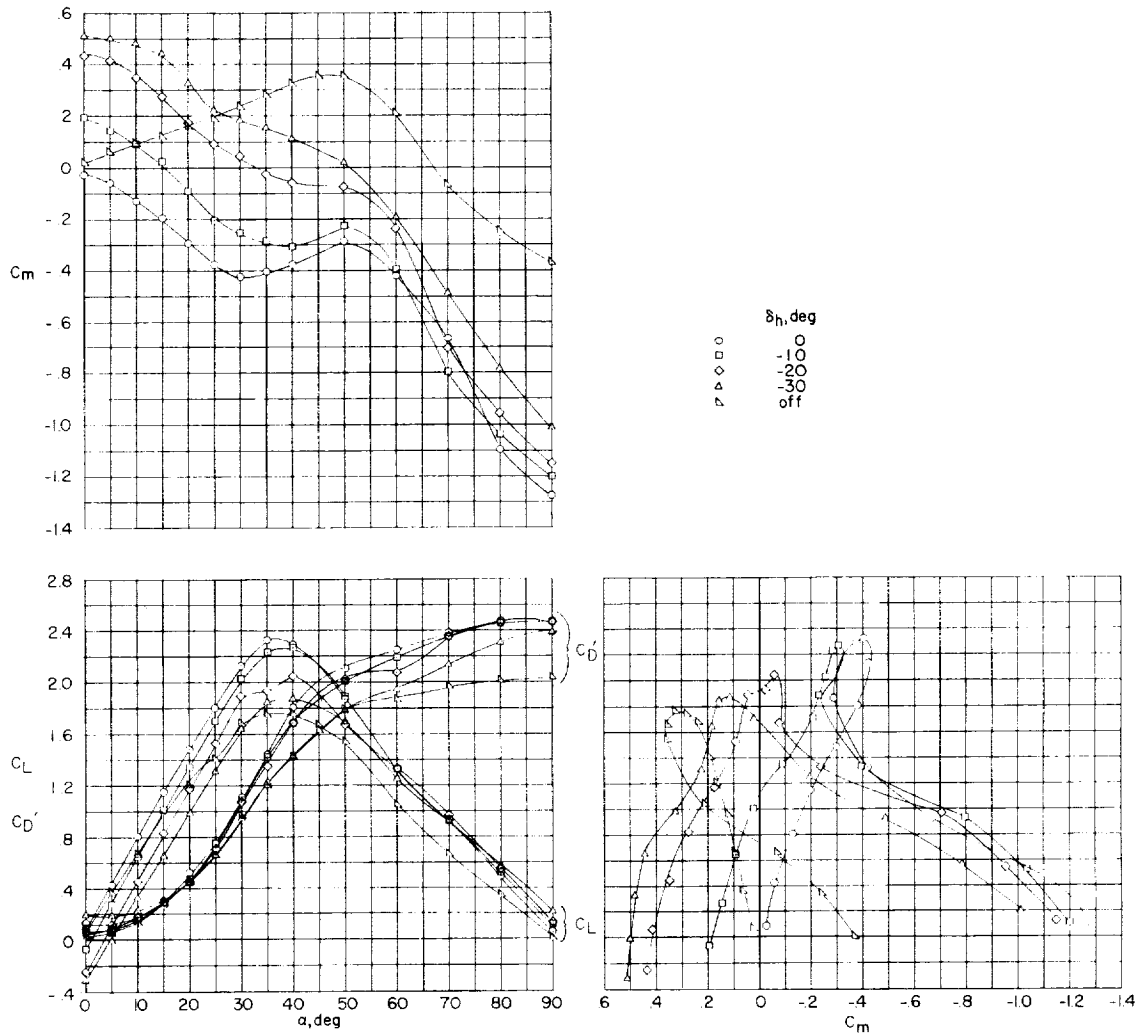
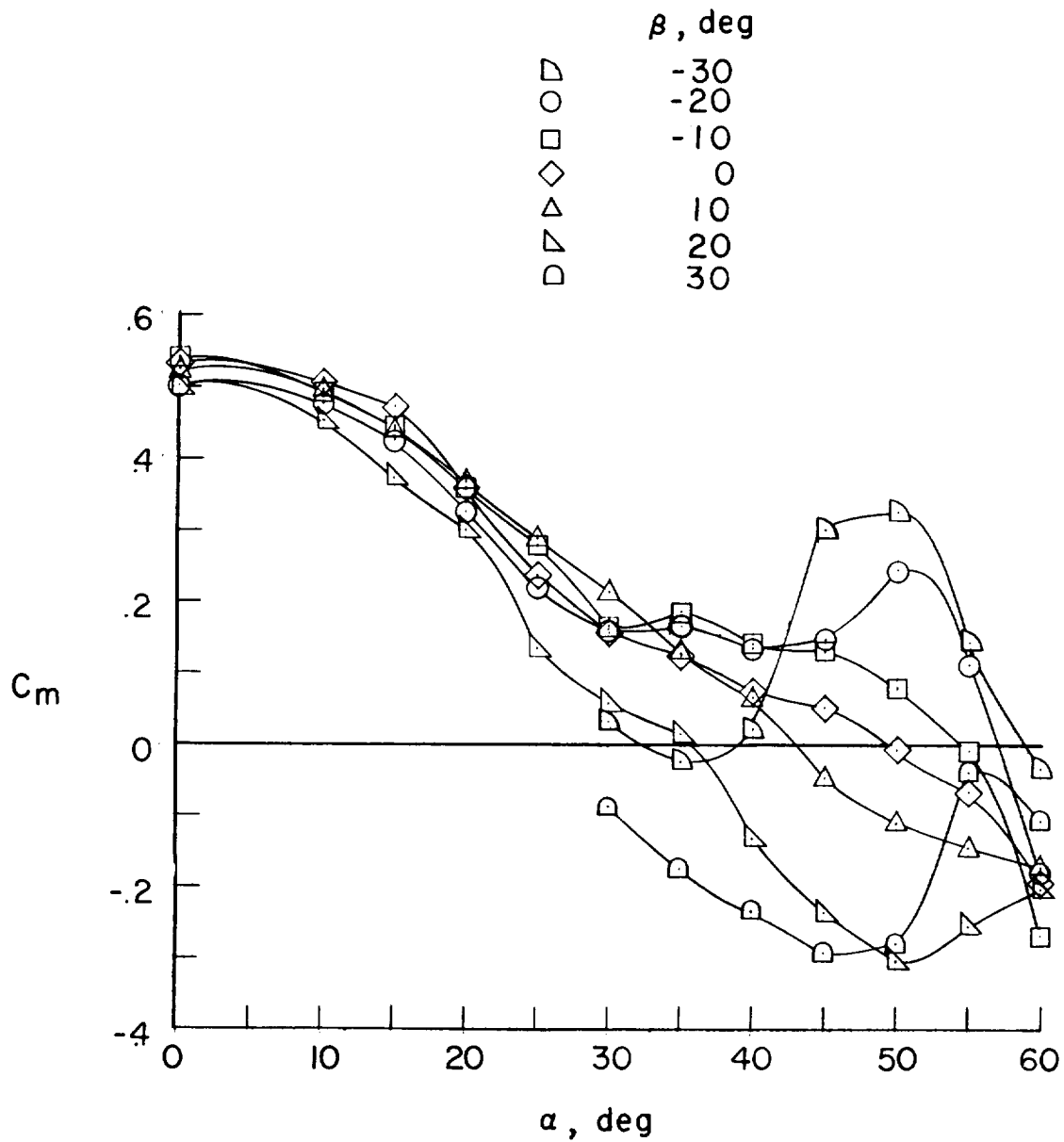


Figure 10.- Photograph of tracking unit. L-57-2267



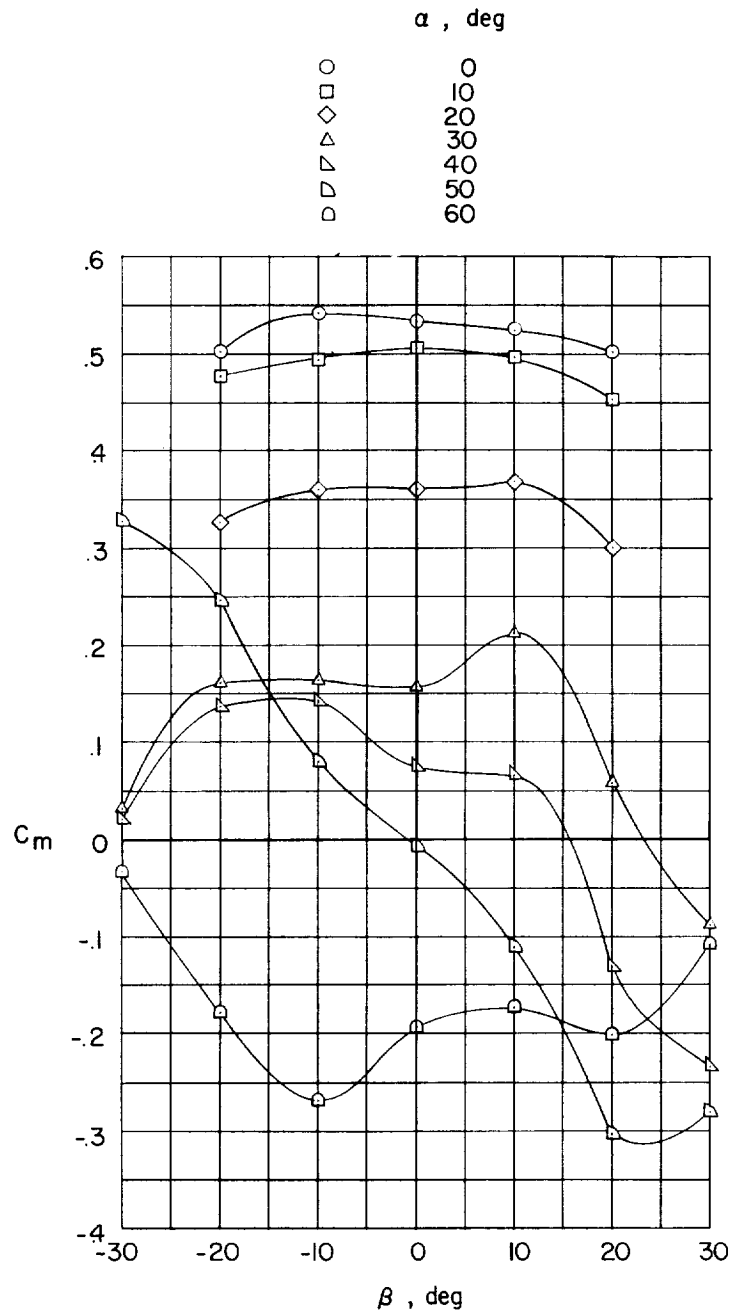
(a) Static longitudinal data.  $\beta = 0^\circ$ . (Derived from data of ref. 2 for center-of-gravity location  $0.21\bar{c}$ .)

Figure 11.- Static longitudinal aerodynamic characteristics of 1/7-scale model of the X-15.



(b) Effect of sideslip angle on  $C_m$  plotted against  $\alpha$ .  $\delta_h = -30^\circ$ .  
(Unpublished data for center-of-gravity location  $0.21\bar{c}$ .)

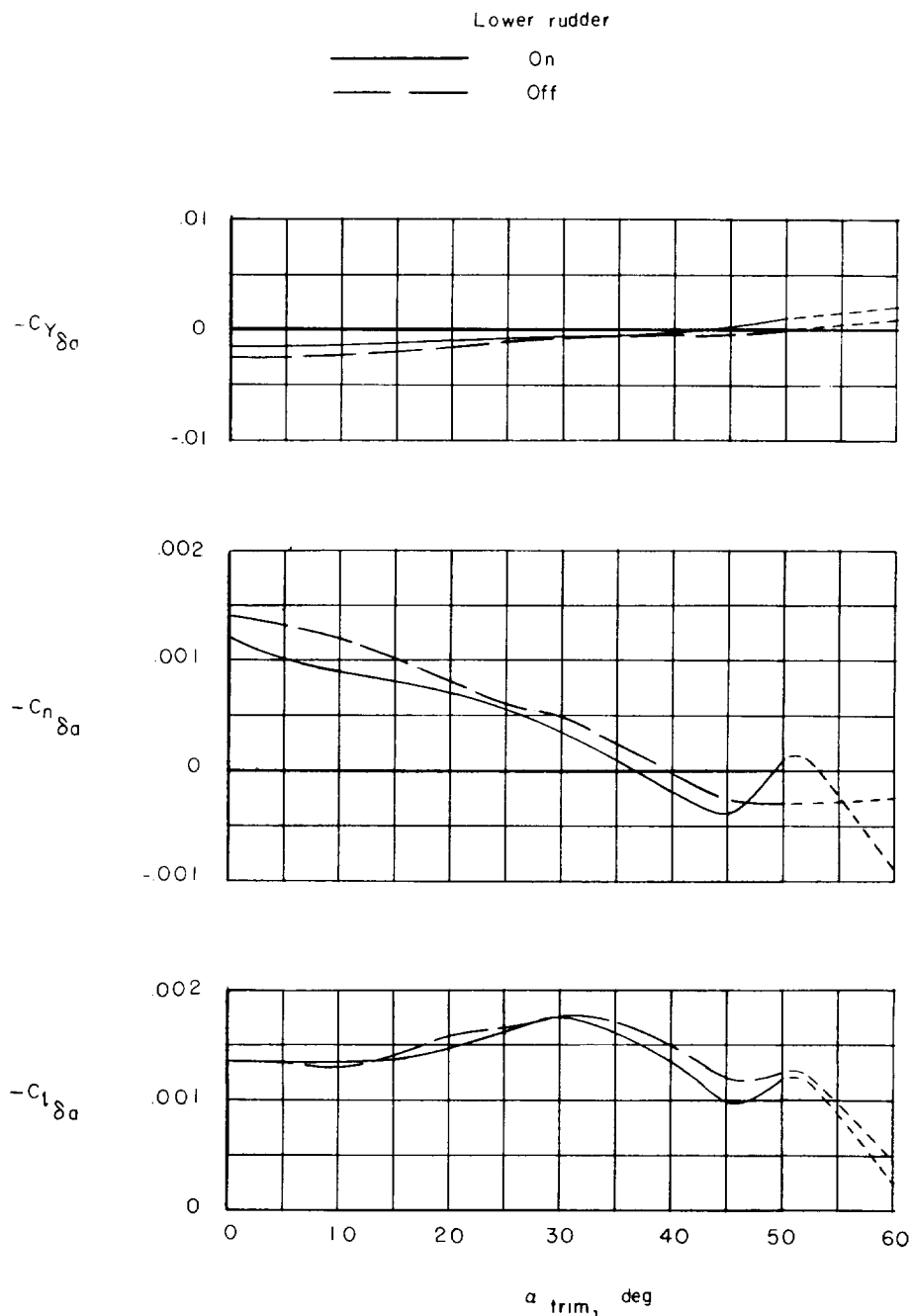
Figure 11.- Continued.



(c)  $C_m$  plotted against  $\beta$ .  $\delta_h = -30^\circ$ . (Unpublished data for center-of-gravity location  $0.21\bar{c}$ .)

Figure 11.- Concluded.

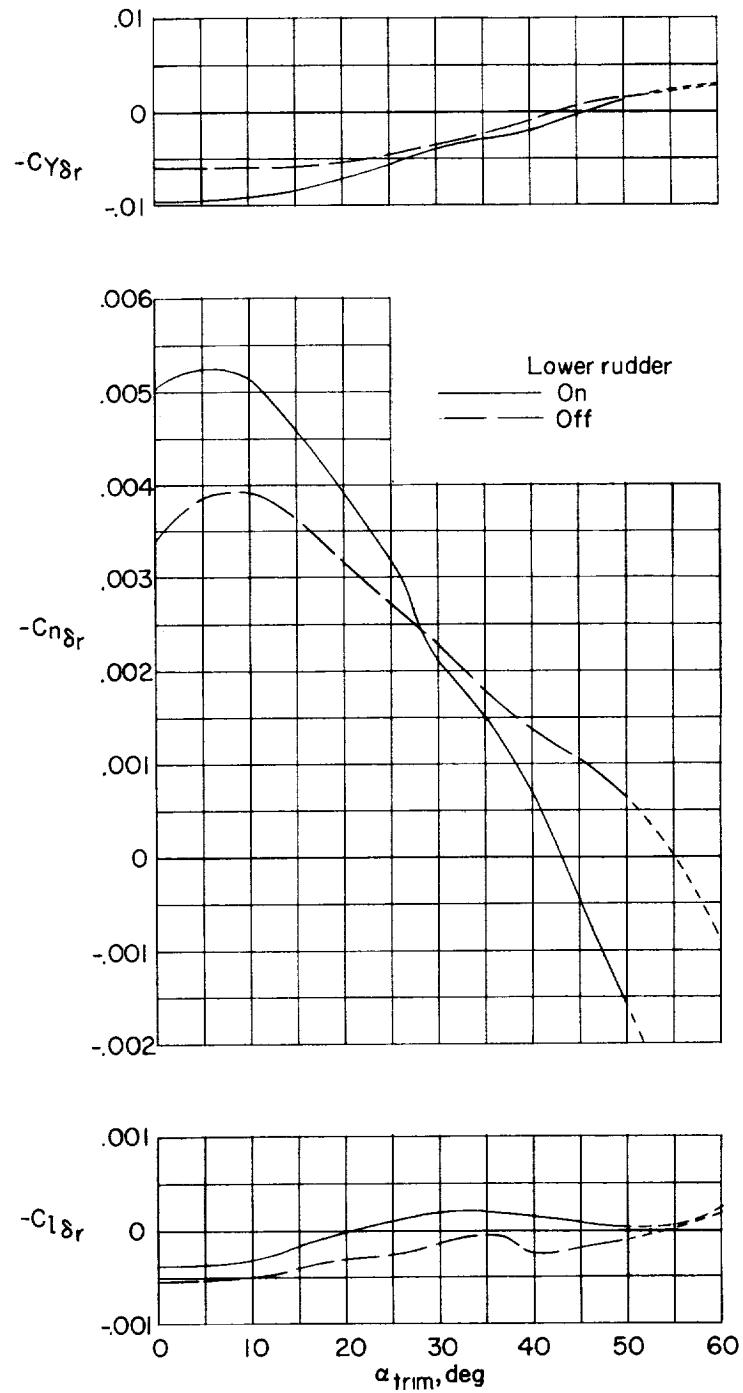




(a) Effectiveness of differentially operated horizontal tails for roll control. (Derived from data of ref. 2.)

Figure 12.- Lateral control effectiveness of 1/7-scale model used in investigation.  $\beta = 0^\circ$ .

[REDACTED]



(b) Rudder effectiveness. (Derived from data of ref. 2.)

Figure 12.- Concluded.

[REDACTED]

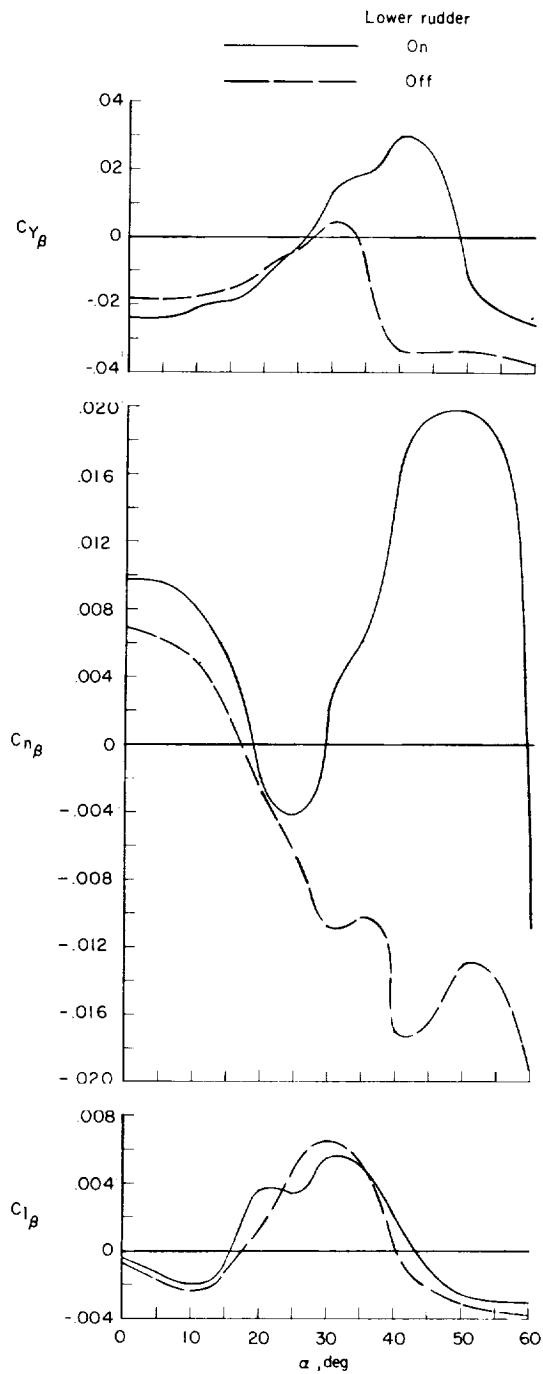


Figure 13.- Variation of the static lateral stability derivatives with angle of attack for the 1/7-scale model of the X-15 (data from ref. 2).

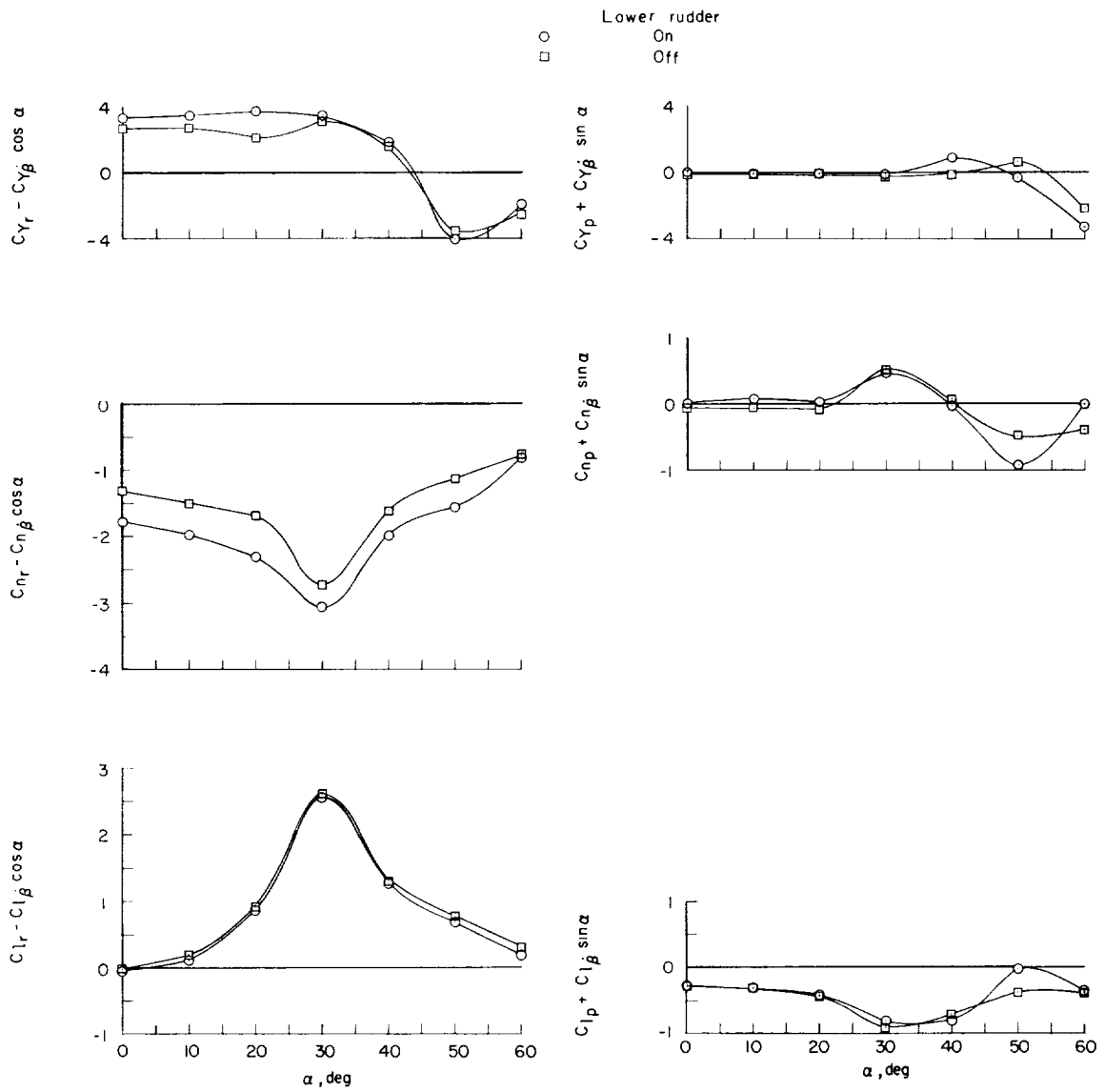


Figure 14.- Variation of the rotary oscillation derivatives with angle of attack for the 1/7-scale model; reduced frequency parameter  $k = 0.105$  (data from ref. 4).



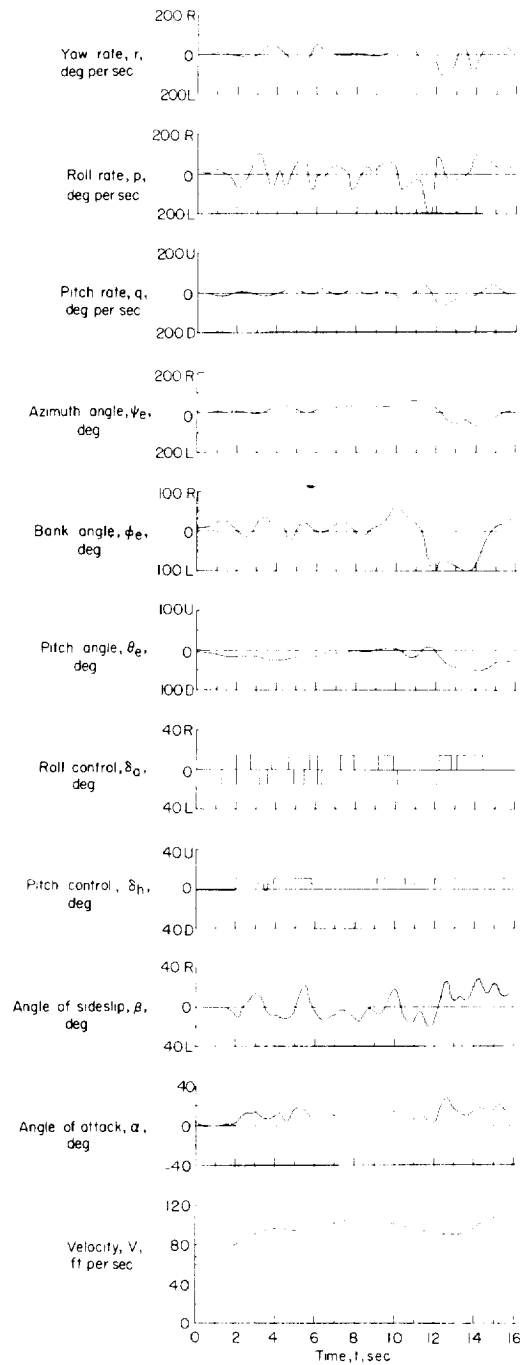


Figure 15.- Time history of flight test A. Lower rudder off, low  $\alpha$  range.

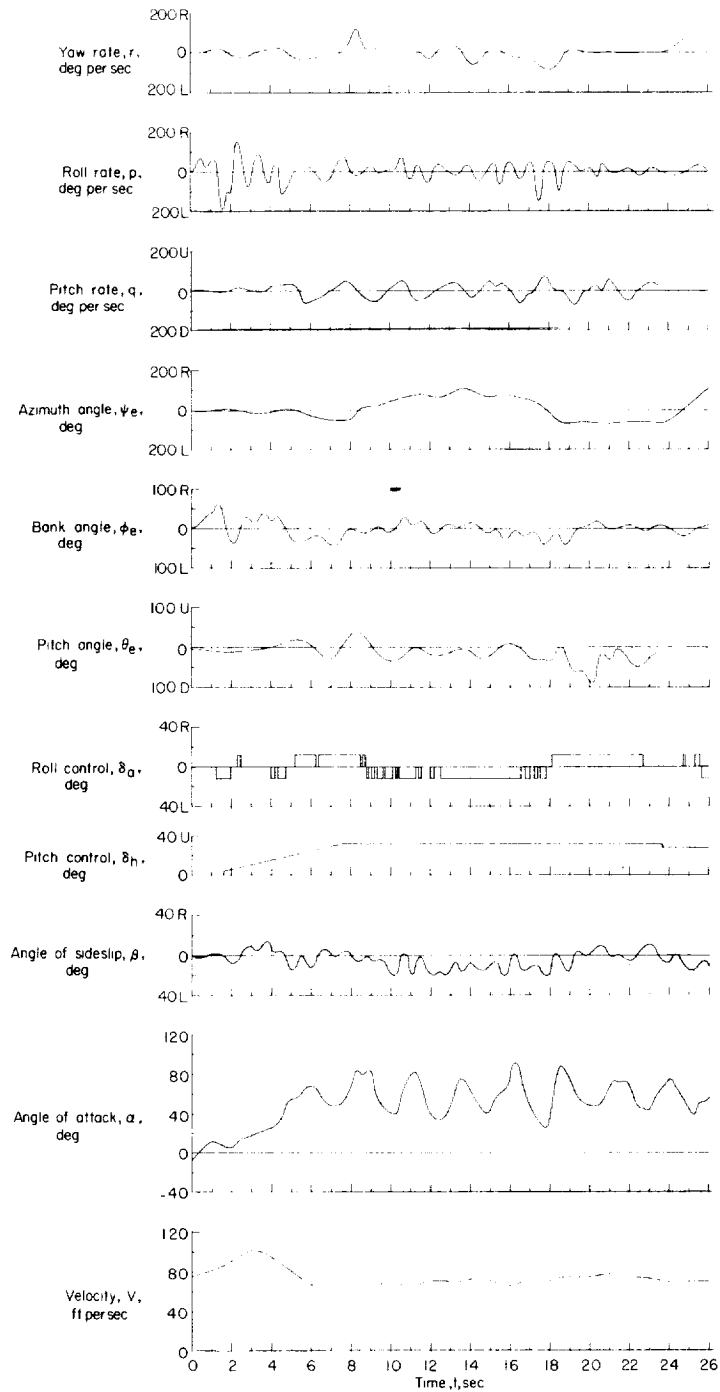
~~CONFIDENTIAL~~

Figure 16.- Time history of flight test B. Lower rudder off, high  $\alpha$  range, no spin.

~~CONFIDENTIAL~~

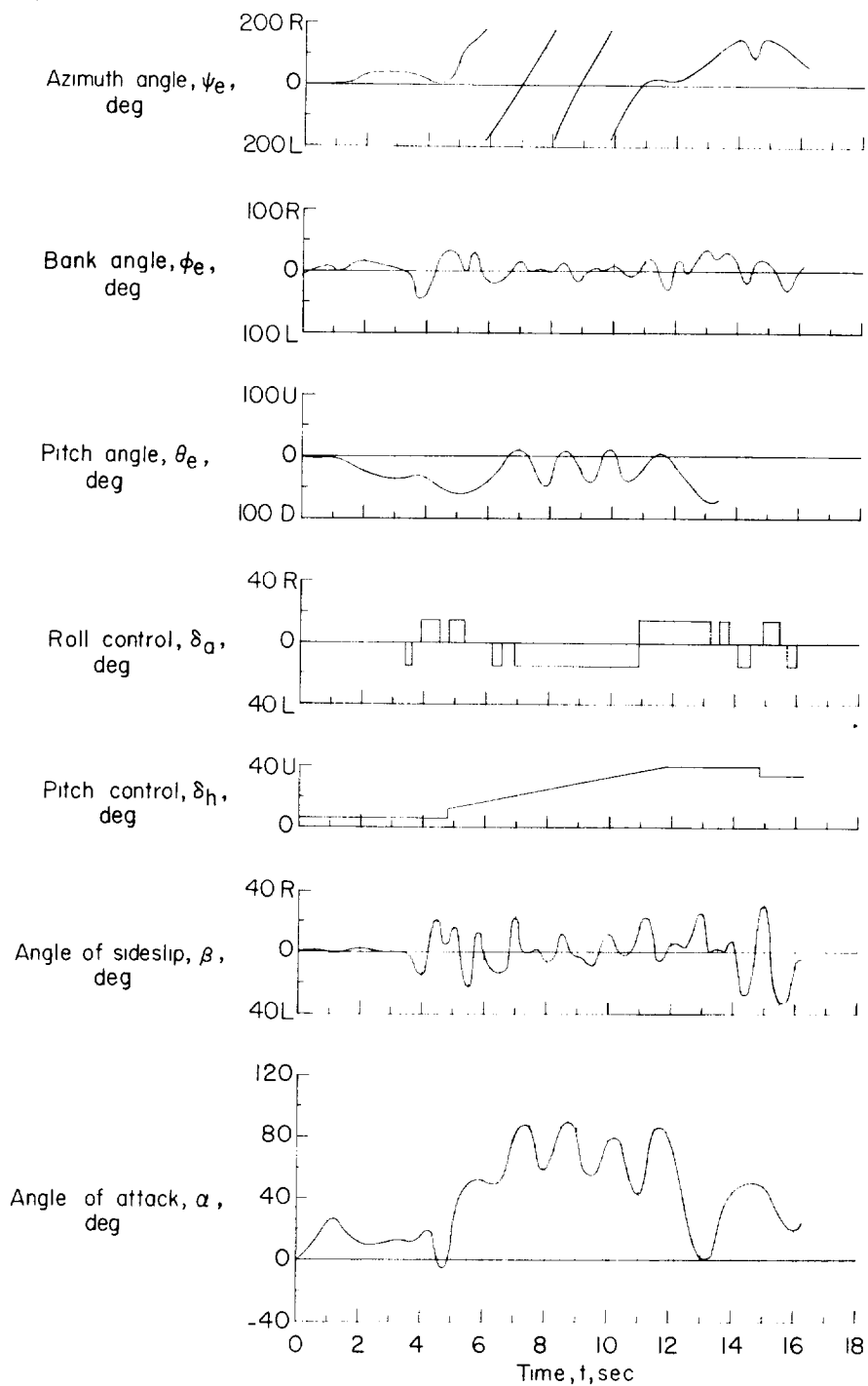


Figure 17.- Time history of flight test C. Lower rudder off, high  $\alpha$  range, incipient spin.

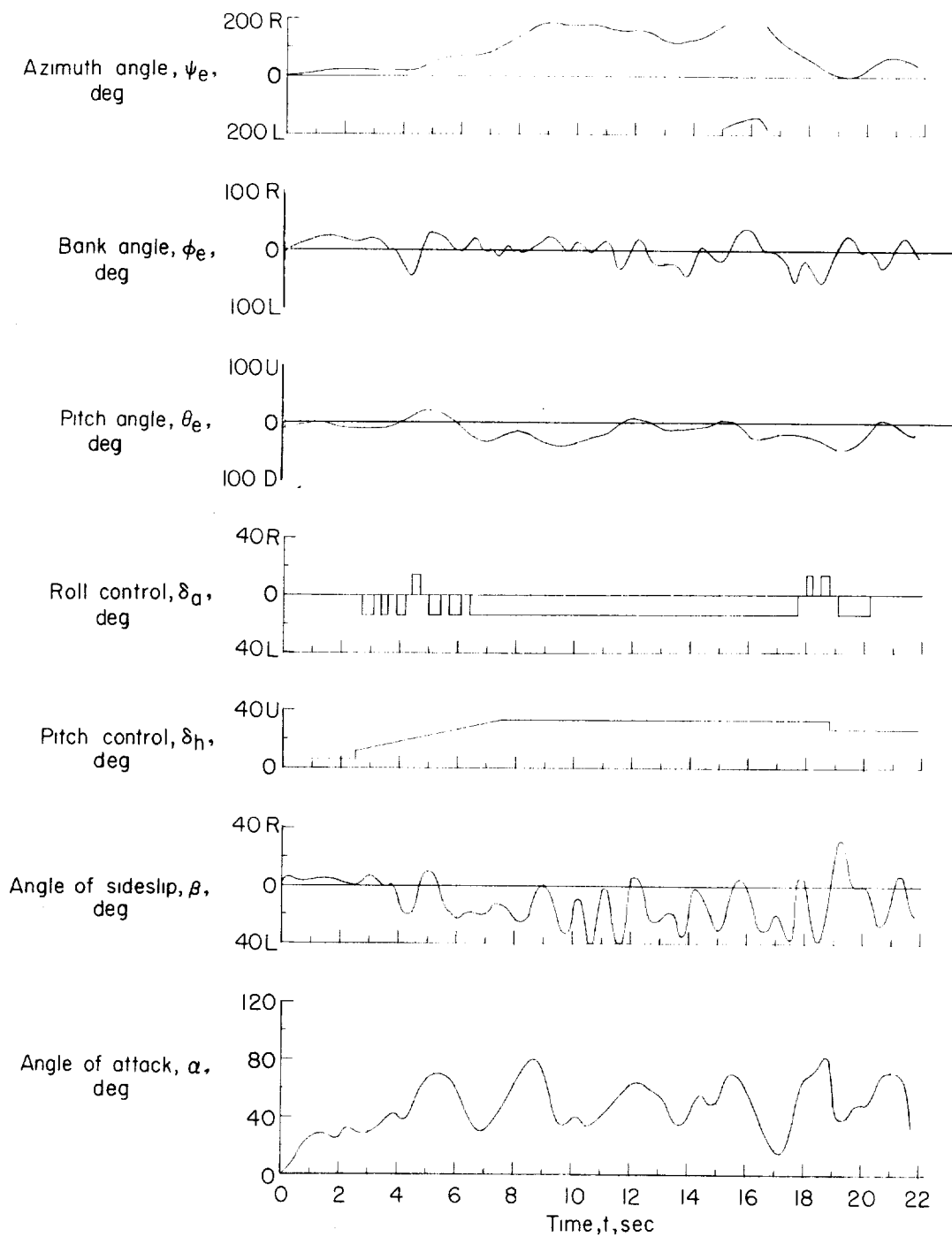


Figure 18.- Time history of flight test D. Complete configuration, high  $\alpha$  range, no spin.

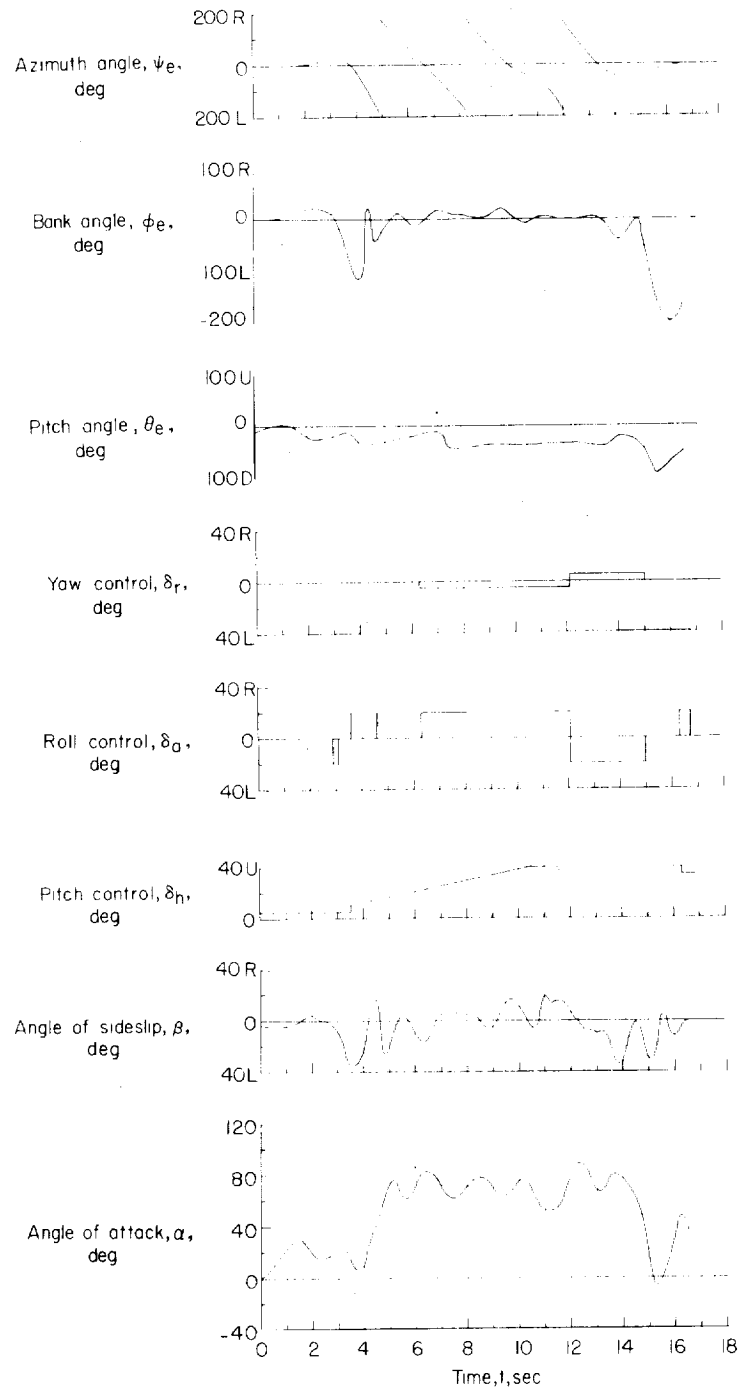
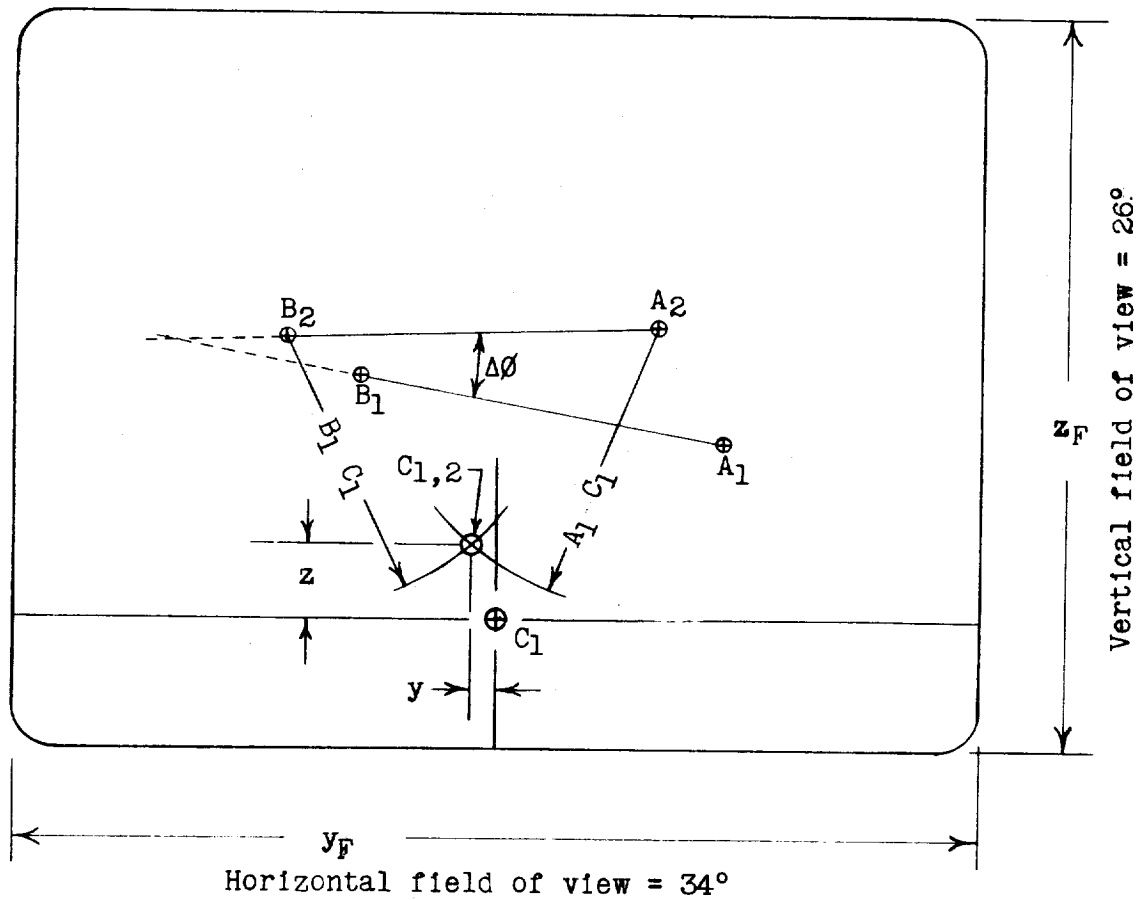


Figure 19.- Time history of flight test E. Complete configuration, high  $\alpha$  range, incipient spin.

CONFIDENTIAL



$$p = \frac{\Delta\phi}{t} = \frac{\Delta\phi}{1/32} = 32 \Delta\phi \text{ deg/sec}$$

$$q = K \frac{z}{t} = K \frac{z}{1/32} = 32Kz \text{ deg/sec}$$

$$r = K \frac{y}{t} = K \frac{y}{1/32} = 32Ky \text{ deg/sec}$$

$$\text{Where } K = \frac{26^\circ}{z_F} = \frac{34^\circ}{y_F} \text{ deg/inch}$$

Figure 20.- Diagram illustrating method for obtaining measurements of p, q, and r from model camera records.

CONFIDENTIAL